Challenge Journal of STRUCTURAL MECHANICS

Vol.11 No.2 (2025)

auxetic buckling load building codes
compressive strength dynamic analysis
earthquake finite element method
girder bridge Jaya algorithm metaheuristic
algorithms modal analysis optimization
prestresing pushover analysis reinforced
concrete seismic design shallow foundations
smart concrete stability static analysis
steel structures structural dynamics
temperature effects thick plate wind

ISSN 2149-8024

TULPAR ACADEMIC PUBLISHING

Challenge Journal of Structural Mechanics

E-mail: *cjsmec@challengejournal.com*

Web page: *cjsmec.challengejournal.com*

Tulpar Academic Publishing
www.tulparpublishing.com

Challenge Journal of Structural Mechanics

CONTENTS

Research Articles

TULPAR ACADEMIC PUBLISHING

Challenge Journal of Structural Mechanics

Research Article

Impact of composite columns on soft and weak storey irregularities in buildings without ground floor infill walls

Yusuf Yıldız [a], Fethi Şermet [a,*]

[a] *Department of Civil Engineering, Iğdır University, 76000 Iğdır, Türkiye*

ABSTRACT

In buildings without infill walls on the ground floor, structural irregularities, such as soft and weak storey irregularities can significantly reduce their resilience to earthquakes. These irregularities arise from insufficient lateral stiffness and strength in the ground floor structure, leading to instability during seismic events. This study investigated the seismic performance of frame structures, focusing on two key factors: the lateral rigidity provided by infill walls and the potential benefits of replacing conventional columns with composite columns on the ground floor. The analysis was conducted in accordance with the Turkish Building Earthquake Code 2018 (TBEC-2018), which provides specific guidelines for designing structures to withstand seismic forces. The findings revealed that including the lateral rigidity of infill walls in the analysis increased the cracked cross-section's moment of inertia by 5%. While this addition enhanced the building's lateral load resistance, it also increased the rigidity irregularity coefficient by 33%, indicating a potential redistribution of seismic forces that could affect the overall stability. On the other hand, introducing composite columns on the ground floor helped reduce the rigidity irregularity coefficient by 20%, providing a more uniform response to lateral loads. However, this improvement came at the cost of a 29% increase in the strength irregularity coefficient, highlighting the challenges in balancing stiffness and strength irregularities. These findings emphasize the importance of carefully evaluating structural modifications to optimize seismic performance. While composite columns are effective in mitigating rigidity irregularities, their impact on strength irregularities must be managed to avoid compromising overall safety.

ARTICLE INFO

Article history:
Received – October 25, 2024
Revision requested – December 30, 2024
Revision received – January 13, 2025
Accepted – January 21, 2025

Keywords:
Composite columns
Infill walls
Seismic behavior
Soft and weak story irregularities

Citation: Yıldız Y, Şermet F (2025). Impact of composite columns on soft and weak storey irregularities in buildings without ground floor infill walls. *Challenge Journal of Structural Mechanics*, 11(2), 70–81.

1. Introduction

Earthquakes pose a major risk to 71% of Türkiye's population and affect 66% of the country's land, with over 24,500 kilometers of active fault lines, including 15,000 kilometers along critical areas. This makes designing earthquake resistant buildings a top priority. One of the most common types of damage in earthquake prone areas is what's called soft storey or weak storey damage. This happens when the ground floor of a building is taller and lacks infill walls to make it more functional for commercial use, leading to more horizontal movement during an earthquake. As a result, the building's structural system can suffer significant damage (Fig. 1).

Soft storey buildings are especially vulnerable to collapse in seismic zones because the lower levels have much less rigidity compared to the floors above, causing damage to worsen (Shahsahebi et al. 2020). Design standards like ASCE/SEI 41-17 (2017) consider a storey to be "soft" if its lateral rigidity is less than 70% of the floor above or 80% of the building's average rigidity.

* *Corresponding author*. Tel.: +90-476-223-0040 ; E-mail address: fethi.sermet@igdir.edu.tr (F. Şermet)
ISSN: 2149-8024 / DOI: https://doi.org/10.20528/cjsmec.2025.02.001

For example, in the 1985 Mexico City earthquake, about 8% of building collapses were linked to soft storey issues, and 42% involved corner buildings with both soft storey and torsional irregularities (Meli 1986). Likewise, the 1995 Kobe earthquake caused extensive destruction in buildings with soft storeys (Watanabe 1997). In 2011 Van, Türkiye earthquake, 75% of the 225 buildings with soft storey issues either collapsed or were severely damaged, highlighting the vulnerability of structures with weak ground floors and large differences in rigidity between storeys (Van Earthquake Report 2011a).

Fig. 1. Heavily damaged buildings whose ground storey columns collapsed due to the soft storey in the Van earthquake (Van Earthquake Report 2011b).

To address soft and weak storey issues in buildings, the rigidity differences between floors need to be reduced. Composite columns, which combine steel and concrete, offer more rigidity than regular reinforced concrete columns because of the added strength from the steel. This makes composite columns a great option for the ground floor to help fix these irregularities. Research has shown the structural benefits of composite columns. For example, Yazdi et al. (2021) studied buildings using concrete-filled steel tube (CFT) columns and found that these columns significantly reduced the likelihood of collapse in low to medium seismic areas. This shows that designing multi-storey buildings with composite columns can greatly improve their safety and earthquake resistance. Solak and Orhan (2023) stated that concrete-filled steel composite columns are a type of steel–concrete composite member that combine the excellent compressive strength of concrete with the high tensile strength of steel, offering superior performance compared to conventional bare steel columns and reinforced concrete columns.

In addition to composite columns, researchers have developed several innovative methods to create more flexible soft storeys in buildings. These include using gapped-inclined braces (GIB), hexabraced systems, and mass dampers (like TMDs and GMDs), which have been studied by experts such as Sahoo (2013), Beigi et al. (2015), Hessabi and Mercan (2016), and Fakhouri and Igarashi (2021). These techniques offer new ways to enhance building resilience in earthquake prone areas.

However, these methods tend to be expensive and are more suitable for areas with high earthquake risks. This study aims to find a solution for regions with lower seismic activity by using more traditional steel-concrete composite elements and evaluating how well they can create a flexible, ductile soft storey to prevent the collapse of multi-storey buildings. One of the most commonly used elements is the concrete encased steel composite column (CES). These columns are crucial in medium and high-rise buildings because they provide high load-bearing capacity, strong lateral strength, and good flexibility under earthquake forces (Sakino et al. 2004; Zhang et al. 2018).

CES columns have been extensively studied through numerous studies examining their performance under various conditions, including axial loads and a combination of axial and lateral forces. For example, a study conducted by Şermet et al. (2021) analyzed the behavior of concrete-encased steel composite column-reinforced concrete beam elements under cyclic seismic forces. The results showed that the composite elements increased ductility and improved the lateral displacement capacity of the structure without significant strength loss, thus increasing its seismic resistance.

In recent years, several studies (Hashemi et al., 2017a, 2017b; Elkady and Lignos 2018) have investigated the collapse mechanisms of multi-storey buildings through large-scale tests under realistic loading scenarios. However, limited research has focused specifically on addressing soft storey irregularities caused by composite columns in medium to high-rise structures. The objective of this study is to determine whether using steel-embedded composite columns solely at the ground floor level can reduce the soft or weak storey irregularities commonly observed in reinforced concrete buildings. For this purpose, a structural system consisting of composite columns on the ground floor and regular reinforced concrete columns on the upper floors was modeled, and its behavior under lateral loads was analyzed.

The analysis varied the ground floor height by 300, 350, 400, 450, 500 and 550 cm and considered various structural scenarios. These included whether the ground

floor columns were made of reinforced concrete or composite materials and whether infill walls were present in the upper storeys. This approach allowed us to examine both the effects of composite columns on soft and weak storey irregularities and to assess the structural response at different ground floor heights. A total of 24 different frame configurations were modeled and analyzed. The ultimate goal of the study is to identify how the use of composite columns in medium to high-rise reinforced concrete buildings influences soft and weak storey irregularities at the ground level, with the aim of proposing an effective solution to mitigate these structural irregularities based on the findings.

2. Materials and Method

Soft and weak floor irregularities are given as B1 and B2 vertical irregularities in the Turkish Building Earthquake Code (TBEC-2018) section 3.6.

2.1. Weak storey irregularity

TBEC-2018 defines a weak storey as one where the strength irregularity coefficient η_{ci} less than 0.80. This coefficient is determined by comparing the total effective shear area of a given storey to that of an upper storey in either of two perpendicular earthquake directions. The calculations for the Strength Irregularity Coefficient are based on Eqs. (1) and (2):

$$\eta_{ci} = (\sum A_e)_i / (\sum A_e)_{i+1} < 0.80 \quad (1)$$

$$(\sum A_e)_i = (\sum A_w)_i + \left(\sum A_g\right)_i + (0.15 \sum A_k)_i \quad (2)$$

Here;
ΣA_e = The effective shear area at any storey in the direction of the earthquake being analyzed [m²].
ΣA_g = It is the total of the cross-sectional areas of the structural system elements that function as a shear wall in the direction aligned with the earthquake being analyzed at any given storey [m²].
ΣA_k = The total area of masonry infill walls (excluding gaps for doors and windows) on any storey that is aligned with the earthquake direction [m²].
ΣA_w = The column cross section at any storey is the total of the effective web areas [m²].

If flexible joints exist between brittle infill walls and frame elements, facade elements are attached to outer frames with flexible connections, or if the infill wall element is separate from the frame, then $A_k = 0$ is selected.

Coefficient of strength irregularity, considering the storey with the lowest value;

a. In the event of $0.60 \leq \eta_{ci} \leq 0.80$ the Structural System Behavior Coefficient from TBEC-2018 Table 4.1 will be multiplied by $1.25(\eta_{ci})$min and applied to all storeys of the building in the direction of both earthquakes.
b. $\eta_{ci} < 0.60$ will never exist.
c. If $\eta_{ci} < 0.60$, the earthquake calculation will be repeated by increasing the strength and rigidity of the weak storey.

2.2. Soft storey irregularity

According to TBEC-2018, a soft storey is identified by calculating the average storey drift ratio at any specified i_{th} storey, excluding basement levels, and dividing this by the average inter-storey drift ratio at a neighboring higher or lower storey, for either of two perpendicular earthquake directions. This assessment shows that the coefficient η_{ki} exceeds 2.0.

The Rigidity Irregularity Coefficient is calculated using Eqs. (3) or (4):

$$\eta_{ki} = \left(\Delta_i^{(x)}/h_i\right)_{\text{avg}} / \left(\Delta_{i+1}^{(x)}/h_{i+1}\right)_{\text{avg}} > 2.0 \quad (3)$$

$$\eta_{ki} = \left(\Delta_i^{(x)}/h_i\right)_{\text{avg}} / \left(\Delta_{i-1}^{(x)}/h_{i-1}\right)_{\text{avg}} > 2.0 \quad (4)$$

Here;
h_i = The storey height of the i_{th} storey of the building [m].
$\left(\Delta_i^{(x)}\right)_{\text{avg}}$ = Average reduced inter storey drift at the i_{th} storey of the building [m].

The relative storey drifts will be calculated using TBEC-2018 Section 4.7.

2.3. Analysis models

In this study, 2D models were created because they are less complicated and allow for quicker analysis. This makes the calculations and modeling processes much more manageable. When dealing with structures where infill walls are present only on the upper floors and not on the ground floor, using a 2D model provides an effective, simplified way to better understand the building's overall rigidity and how it would behave during an earthquake.

In the analyses, a detailed 2D frame model was developed, consisting of a ground floor designed as a soft storey beneath five standard upper storeys, as illustrated in Fig. 2. This configuration allowed for a focused examination of soft storey behavior, especially in relation to varying ground floor heights and their impact on structural irregularities.

The model was designed to evaluate the impact of varying ground floor heights on the overall behavior of the building frame. Six ground floor heights were tested: 300, 350, 400, 450, 500, and 550 cm, providing a range to analyze how increased heights influence the stability and flexibility of the structure. To ensure consistency, the height of each upper floor was fixed at 300 cm, allowing any observed performance differences to be directly linked to changes in the ground floor. The ground floor was modeled without infill walls to simulate the soft floor effect typical in designs requiring open spaces, such as parking areas or lobbies. In contrast, all upper floors, including balconies, were constructed with infill walls to represent typical multi-storey building conditions. These walls add rigidity to the upper floors, further highlighting the ground floor's flexibility and providing clear insights into how the structure responds to loads differ-

ently across its height. This configuration enables a focused analysis of how varying ground floor heights influence the building's performance under lateral forces like wind or earthquakes.

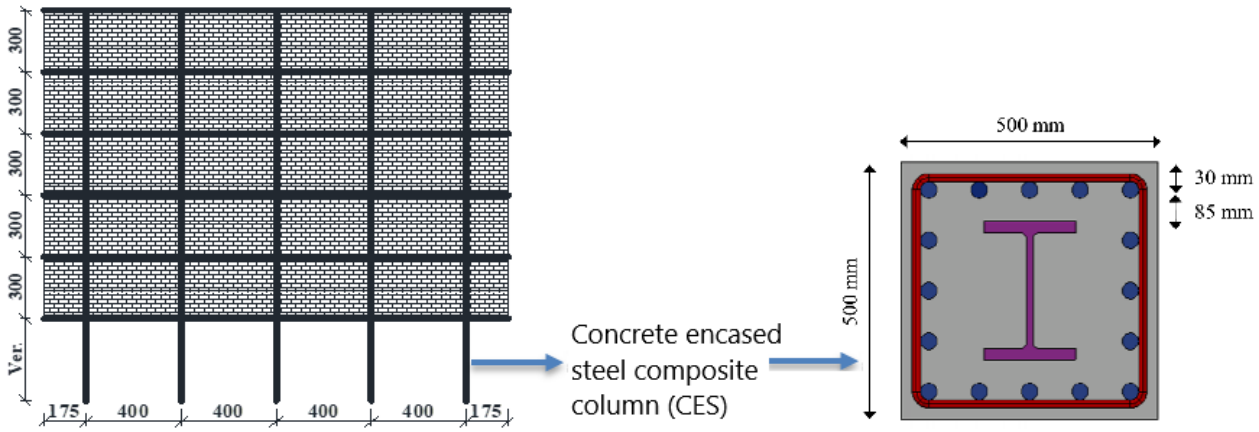

Fig. 2. Frame analysis model.

The model includes reinforced concrete columns sized 50x50cm and beams sized 25x50cm. For composite columns, the HE240M steel profile is used. The structural elements are made from C30/37 grade concrete and S275 grade steel, ensuring the model accurately represents commonly used construction materials. Pumice concrete blocks are used for the infill walls. The loading conditions are set as follows: a dead load (G) of 0.575 tf/m is applied to all beams, and live loads (Q) are set at 0.20 tf/m for interior beams and 0.50 tf/m for cantilever beams. The load from the infill walls is 0.35 tf/m.

The study explores six different ground floor heights 300, 350, 400, 450, 500, and 550 cm resulting in a total of 24 unique model variations. Table 1 summarizes the main features, groupings, and abbreviations for each of these models, making it easy to compare and understand their different configurations.

Table 1. Summary of the analyzed models.

No.	Ground storey height (cm)	Ground storey with RC. col. models	Ground storey with RC. col. and wall rigidities included	Ground storey with composite column models	Ground storey with C. col. and wall rigidities included
		Group 1	Group 2	Group 3	Group 4
1	300	B300C	B300D	C300C	C300D
2	350	B350C	B350D	C350C	C350D
3	400	B400C	B400D	C400C	C400D
4	450	B450C	B450D	C450C	C450D
5	500	B500C	B500D	C500C	C500D
6	550	B550C	B550D	C550C	C550D

2.4. Earthquake parameters and design information

The two-dimensional frame analysis uses specific earthquake parameters to assess the structural response to seismic forces. These earthquake parameters, detailed in Table 2, include essential factors such as the seismic zone, soil type, peak ground acceleration (PGA), and response modification factors. These factors are selected based on regional seismic standards to simulate realistic earthquake loading conditions that the building might experience. By applying these parameters, the model provides insights into how the structure's stiffness and stability would perform under potential earthquake scenarios.

Along with the earthquake parameters, the specific design details of the building's structural elements are outlined in Table 3. This table provides clear specifications for key features, such as material strengths, column and beam dimensions and reinforcement details. It also covers the layout of the structural system, including how beams connect to columns, the base of each column, and any special reinforcements added for better flexibility under stress.

These details help ensure that the model closely resembles real construction practices, leading to accurate and dependable simulation results that can guide structural assessments. Together, Tables 2 and 3 give a complete picture of both the earthquake forces the building is designed to withstand and the structural elements that help it do so. This combined information allows for a well-rounded evaluation of how the building would likely respond to seismic events.

Table 2. Earthquake parameters.

Building location			
Latitude	41.059128	Longitude	28.968130
Map spectral acceleration coefficients			
S_S	0.825	S_1	0.239
S_{DS}	0.990	S_{D1}	0.359
PGA	0.340	PGV	21.946

Table 3. Design information.

Building usage classification	3	Earthquake design class	1
Building importance level	1	Building height class	5
Seimic ground motion level	DD-2	Normal performance target	Controlled damage
Evaluation/design approach	Strength based design	Slab type	Beam slab
Ductility level	High	Rx/Dx	8/3
Diaphragm type	Rigid		
Ground class	ZC	Density of soil	2.10 tf /m^3
Bearing capacity of soil	20 tf /m^2	Coefficient of soil reaction	2,400 tf /m^3

2.5. Software

ideCAD Static is a comprehensive professional Structural BIM software specifically developed for modeling, finite element analysis, code-compliant design, performance evaluation and strengthening of structural systems. Earthquake loads were determined using ideCAD Static v.10.20, following the Equivalent Earthquake Load Method and the Linear Earthquake Calculation principles outlined in Section 4.7 of TBEC-2018.

CSiCol is a comprehensive software package used for the analysis and design of columns, effectively addressing the design of columns in any type of concrete, reinforced concrete or composite sections. CsiCol was used to determine the composite column sections.

2.6. Method for calculating wall rigidity

It has been observed that infill walls significantly increase the rigidity of the structure and cause a noticeable reduction in the building period (Zengin 2021). In this study, the infill walls are not represented in the analytical model as an equivalent diagonal strut with hinged ends, as is commonly done in the literature. Instead, a more practical approach is taken by mathematically incorporating them into the effective lateral rigidity of the storey through the use of moments of inertia and modulus of elasticity. Macro modelling of infill walls with equivalent struts can be seen in Fig. 3.

TBEC-2018 does not consider the rigidity of infill walls when assessing soft storey irregularities. However, it is evident that rigidly connected infill walls, which account for 15% of the strength in weak storey calculations, will still influence soft storey irregularity to some extent based on their stiffness. Therefore, in the calculations for soft storey irregularities, the rigidity of the infill walls is set at 5% instead of 15%, reflecting a value equivalent to the moment of inertia of the cracked cross-section (Tezcan et al. 2007). The modulus of elasticity for the walls was determined using Eq. 5, developed with the FlatJack Method (Ulukaya and Yüzer 2017).

$$E_w = 0.11.E_h^{1.35}.E_t/(1.84.E_h + E_t) \quad (5)$$

Here;
E_h = The elasticity modulus of the mortar [MPa].
E_t = Wall elasticity modulus [tf /cm^2].

The modulus of elasticity for the wall binder mortar was determined using Equation 12.1 from the Regulation on Design, Calculation, and Construction Principles of Steel Structures (TSC). The elasticity formula for masonry mortar is presented in Eq. (6).

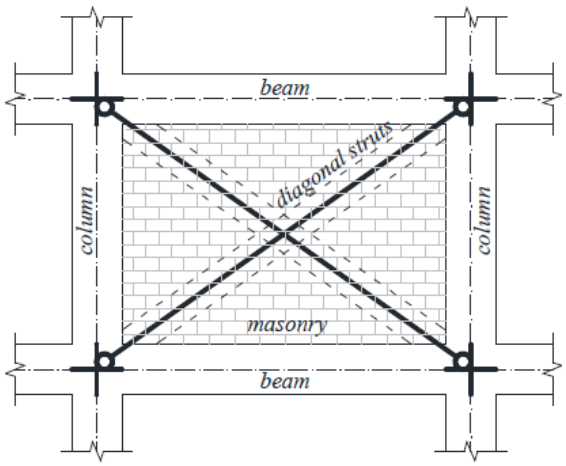

Fig. 3. Macro modelling of infill walls with equivalent struts (Lima and Martinelli 2014).

$$E_c = 0.043.w_c^{1.5}.\sqrt{f_{ck}} \quad (6)$$

Here;
w_c = The density of the mortar [kg /m³].
f_{ck} = Characteristic compressive strength of the mortar [MPa].

The modulus of elasticity (E_t) for pumice concrete block infill walls is determined to be 70 tf/cm², with the characteristic strength of the mortar at 8 MPa and a density of 2,000 kg/m³. According to TBEC-2018, the effective bending rigidity factor for the walls was accepted as 0.50, as indicated in Table 4.2. The effective lateral drift rigidity of the walls (k_w) was calculated using Eq. (7), excluding the lateral drift rigidity of the walls on the cantilever beams.

$$k_{wx} = (12.E_w.I_{wx})/h^3 \quad (7)$$

2.7. Composite column design approach

For this study, CES composite columns was chosen, where a steel section is surrounded by reinforced concrete, are extensively used as key load-bearing components in high-rise structures. In accordance with TSC Section 12.3.1.5(a), the distance between the steel core and the nearest longitudinal rebar must be at least 1.5 times the diameter of the rebar and no less than 40 mm. The HEM240 profile, which has the largest cross-section meeting these criteria, was selected.

When determining the material properties of the composite column, the modulus of elasticity was calculated based on the Poisson ratio and the unit weight ratios of concrete and steel. The effective cross-sectional areas were then derived from the ratio of the elastic modulus using Eqs. (8–11).

$$E_{comp} = E_c.V_c + E_s.V_s \quad (8)$$

$$\upsilon_{comp} = \upsilon_c.V_c + \upsilon_s.V_s \quad (9)$$

$$w_{comp} = w_c.V_c + w_s.V_s \quad (10)$$

$$A_{comp} = A_c - A_s + r_{Esc}.A_s \quad (11)$$

Here;
$E_{comp,c,s}$ = Elastic modulus of composite section, considering concrete and steel [tf /m²].
$\upsilon_{comp,c,s}$ = Poisson ratios of composite section, considering concrete and steel.
$w_{comp,c,s}$ = Density of composite section, considering concrete and steel [tf /m³].
$A_{comp,c,s}$ = Areas of composite section, considering concrete and steel [cm²].
$V_{c,s}$ = Concrete and steel volume ratios.
r_{Esc} = The ratio of the modulus of elasticity of steel to that of concrete.

The HE240M profile is placed within the reinforced concrete column, with its body aligned parallel to the frame direction (along the x direction). Material and cross-sectional properties were determined using the CSiCol v.10 program, minimizing reinforcement contributions. These values from CSiCol v.10 were then input into ideCAD Static v.10.20, where they were linearly analyzed using the equivalent earthquake load method. Earthquake loads were calculated, and irregularity assessments were conducted. The cross-section of the composite column is shown in Fig. 4, with its properties listed in Table 4.

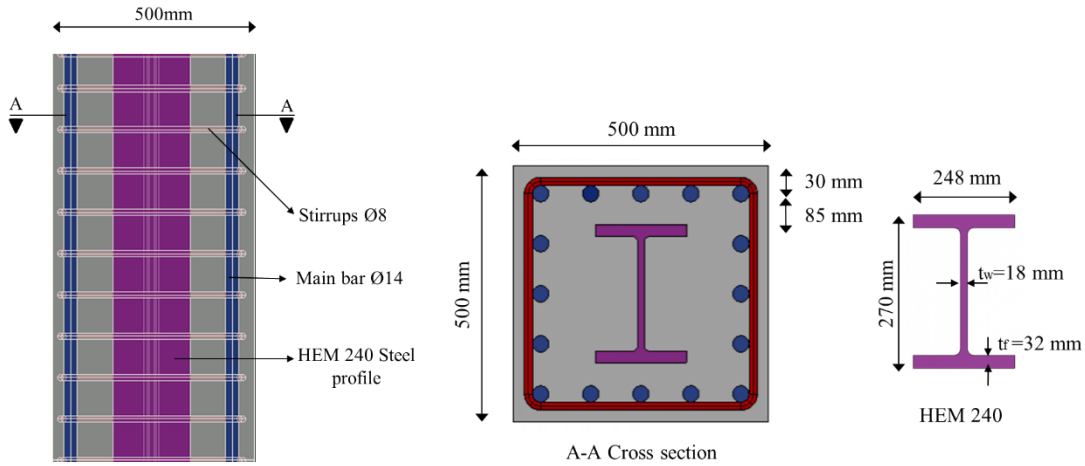

Fig. 4. Longitudinal and cross-section of the composite column.

Table 4. Properties of the composite column cross-section.

Modulus of elasticity (tf/m²)	4,544,000.00	Cross-sectional area (cm²)	3,573.85
Poisson's ratio	0.21	Shear area – SA_2 (cm²)	3,167.81
Density (tf/m³)	2.93	Shear area – SA_3 (cm²)	2,501.20
Moment of inertia – I_{22} (cm⁴)	651,418.10	Moment of inertia – I_{33} (cm⁴)	564,572.06

Note: Since the methods in this study are designed for buildings without infill walls on the ground floor, the irregularities in the storeys above the ground floor are not examined.

3. Results and Discussion

3.1. Soft storey irregularity controls

In models with reinforced concrete columns, increasing the height of the ground storey results in a decrease in column rigidity, which contributes to the formation of soft storey irregularities. As the ground storey height rises, columns become less rigid, making the structure more susceptible to lateral displacements during an earthquake. This reduction in rigidity can lead to soft storey behavior, a condition in which one storey is significantly more flexible than the others, affecting the building's overall stability. To quantify this effect, the soft storey irregularity coefficient (η_{ki}) was calculated for each storey using Eqs. (3) and (4), with results shown in Tables 5–12. The analysis of the 1st Group models, based on TBEC-2018 Section 3.6, initially focused on detecting these irregularities in the ground storey. According to these results, soft storey irregularities appeared in models with ground storey heights of 450 cm or greater, where columns reduced rigidity led to irregularity.

In Tables 5 and 6, soft storey irregularities are marked, with 'None' indicating no irregularities and 'Yes' indicating their presence. These findings illustrate the importance of controlling ground storey height to prevent soft storey conditions, as increased height directly impacts lateral rigidity and the building's earthquake resilience.

Table 5. Group 1 soft storey irregularity controls.

Storey No.	B300C			B350C			B400C		
	η_{ki}(+)	η_{ki}(-)	Control	η_{ki}(+)	η_{ki}(-)	Control	η_{ki}(+)	η_{ki}(-)	Control
5	–	0.48	None	–	0.48	None	–	0.48	None
4	2.07	0.71	Yes	2.07	0.71	Yes	2.07	0.70	Yes
3	1.41	0.82	None	1.42	0.82	None	1.42	0.81	None
2	1.22	0.89	None	1.22	0.89	None	1.23	0.89	None
1	1.12	0.95	None	1.12	0.69	None	1.13	0.53	None
Z	1.05	–	None	1.45	–	None	1.90	–	None

Table 6. Group 1 soft storey irregularity controls (continued).

Storey No.	B450C			B500C			B550C		
	η_{ki}(+)	η_{ki}(-)	Control	η_{ki}(+)	η_{ki}(-)	Control	η_{ki}(+)	η_{ki}(-)	Control
5	–	0.48	None	5	–	0.48	None	5	–
4	2.07	0.70	Yes	4	2.07	0.70	Yes	4	2.07
3	1.42	0.81	None	3	1.42	0.81	None	3	1.42
2	1.23	0.88	None	2	1.23	0.88	None	2	1.23
1	1.13	0.41	None	1	1.13	0.41	None	1	1.13
Z	2.43	–	Yes	Z	2.43	–	Yes	Z	2.43

The lateral drift rigidity of the wall, calculated as 85.28 tf/cm from the analysis, was incorporated into the effective drift rigidity of the ground storey in the second group of analysis models, as presented in Table 1. By adding this wall rigidity component, the models were then examined for soft storey irregularities, focusing on whether this added rigidity affected the ground storey's stability across varying heights.

Soft storey irregularities were identified in models with ground storey heights of 400 cm and above, indicating a noticeable impact of the wall's added rigidity on the structural behavior. Specifically, the inclusion of wall lateral drift rigidity led to an approximately 33% increase in the rigidity irregularity coefficient for the ground storeys across all tested heights, when compared to the results from the first group analysis models where wall rigidity was not accounted for.

A clear difference was observed between the two groups of models: in the first group, where wall stiffness was excluded, soft storey irregularities only began to appear at a ground storey height of 450 cm. However, in the second group, where wall stiffness was included in the calculations, these irregularities appeared at the lower height of 400 cm. This suggests that the added lateral drift rigidity from the walls amplified the stiffness irregularity coefficient, making the structure more prone to soft storey irregularities even at reduced ground storey heights.

These results, as shown in Tables 7 and 8, highlight the importance of considering wall rigidity in structural designs, as it plays a crucial role in the seismic performance and stability of buildings with varying ground storey heights.

Table 7. Group 2 soft storey irregularity controls.

Storey No.	B300C			B350C			B400C		
	η_{ki}(+)	η_{ki}(-)	Control	η_{ki}(+)	η_{ki}(-)	Control	η_{ki}(+)	η_{ki}(-)	Control
5	–	0.48	None	5	–	0.48	None	5	–
4	2.07	0.71	Yes	4	2.07	0.71	Yes	4	2.07
3	1.41	0.82	None	3	1.41	0.82	None	3	1.41
2	1.22	0.89	None	2	1.22	0.89	None	2	1.22
1	1.12	0.71	None	1	1.12	0.71	None	1	1.12
Z	1.40	–	None	Z	1.40	–	None	Z	1.40

Table 8. Group 2 soft storey irregularity controls (continued).

Storey No.	B450C			B500C			B550C		
	η_{ki}(+)	η_{ki}(-)	Control	η_{ki}(+)	η_{ki}(-)	Control	η_{ki}(+)	η_{ki}(-)	Control
5	–	0.48	None	5	–	0.48	None	5	–
4	2.07	0.70	Yes	4	2.07	0.70	Yes	4	2.07
3	1.42	0.81	None	3	1.42	0.81	None	3	1.42
2	1.23	0.88	None	2	1.23	0.88	None	2	1.23
1	1.13	0.31	None	1	1.13	0.31	None	1	1.13
Z	3.23	–	Yes	Z	3.23	–	Yes	Z	3.23

In the third group of analysis models (Table 1), the effect of using composite columns on the ground floor was investigated to assess their effectiveness in reducing the soft story irregularity. This assessment was based on the criteria outlined in Section 3.6 of TBEC-2018, which states that the wall lateral drift stiffness is not included in the analysis.

The results of the calculations indicated a significant improvement in structural performance; specifically, the stiffness irregularity coefficient for models featuring composite columns in the ground storey was found to be approximately 20% lower than that of the first group analysis models, which did not take wall lateral drift rigidity into account. This reduction suggests that the incorporation of composite columns enhances the overall stability of the structure by effectively addressing issues related to soft storey irregularity.

Further analysis revealed that the soft storey irregularity was particularly pronounced at a ground storey height of 500 cm. This finding emphasizes the importance of height considerations in structural design, particularly in seismic zones where soft storey irregularity can lead to significant vulnerabilities. The detailed results of this analysis, including comparative data and specific findings, are thoroughly documented in Tables 9 and 10, providing a comprehensive overview of the effectiveness of composite columns in reducing soft storey irregularity in the ground storey.

Overall, these findings contribute valuable insights into the design practices for tall structures, particularly in regions subject to seismic activity, highlighting the role of composite columns in enhancing structural integrity and performance.

Table 9. Group 3 soft storey irregularity controls.

Storey No.	B300C			B350C			B400C		
	η_{ki}(+)	η_{ki}(-)	Control	η_{ki}(+)	η_{ki}(-)	Control	η_{ki}(+)	η_{ki}(-)	Control
5	–	0.48	None	5	–	0.48	None	5	–
4	2.07	0.71	Yes	4	2.07	0.71	Yes	4	2.07
3	1.41	0.82	None	3	1.41	0.82	None	3	1.41
2	1.22	0.89	None	2	1.22	0.89	None	2	1.22
1	1.12	1.18	None	1	1.12	1.18	None	1	1.12
Z	0.84	–	None	Z	0.84	–	None	Z	0.84

Table 10. Group 3 soft storey irregularity controls (continued).

Storey No.	B450C			B500C			B550C		
	η_{ki}(+)	η_{ki}(-)	Control	η_{ki}(+)	η_{ki}(-)	Control	η_{ki}(+)	η_{ki}(-)	Control
5	–	0.48	None	5	–	0.48	None	5	–
4	2.07	0.70	Yes	4	2.07	0.70	Yes	4	2.07
3	1.42	0.81	None	3	1.42	0.81	None	3	1.42
2	1.23	0.88	None	2	1.23	0.88	None	2	1.23
1	1.13	0.51	None	1	1.13	0.51	None	1	1.13
Z	1.95	–	None	Z	1.95	–	None	Z	1.95

In the fourth group analysis models, the calculations were re-conducted to incorporate both wall lateral drift rigidity and the integration of composite columns in the ground storey. This dual approach aimed to further enhance the structural performance by addressing two critical aspects of design: the rigidity provided by the walls against lateral drift and the strength characteristics of composite columns.

The results of this comprehensive analysis demonstrated a significant reduction in the stiffness irregularity coefficient, which decreased by approximately 20% compared to the second group analysis models. The second group had already included ground storey reinforced concrete columns along with wall lateral drift rigidities; thus, the additional benefits of using composite columns highlight their effectiveness in enhancing the overall stability and rigidity of the structure.

Soft storey irregularity was specifically noted at a ground storey height of 450 cm, indicating that while incorporating composite columns and wall lateral drift rigidity improved performance, certain height configurations still posed challenges related to soft storey irregularity. This observation underscores the importance of carefully considering storey heights during the design process, as variations can influence the structural response under lateral loads.

The detailed findings from this analysis are systematically presented in Tables 11 and 12, which provide a thorough breakdown of the numerical data and comparative results between the different model groups. These tables serve as a vital resource for understanding the implications of incorporating both composite columns and wall lateral drift rigidity in structural design, particularly in relation to mitigating soft storey irregularities.

Ultimately, the insights gained from this fourth group analysis contribute to the broader discourse on optimizing building design for resilience against lateral forces, such as those encountered during seismic events. The combination of composite columns with wall lateral drift rigidity emerges as a promising strategy for improving the performance of structures, especially in high-risk areas, and could inform future design standards and best practices in civil engineering.

Table 11. Group 4 soft storey irregularity controls.

Storey No.	B300C			B350C			B400C		
	η_{ki}(+)	η_{ki}(-)	Control	η_{ki}(+)	η_{ki}(-)	Control	η_{ki}(+)	η_{ki}(-)	Control
5	–	0.48	None	5	–	0.48	None	5	–
4	2.07	0.71	Yes	4	2.07	0.71	Yes	4	2.07
3	1.41	0.82	None	3	1.41	0.82	None	3	1.41
2	1.22	0.89	None	2	1.22	0.89	None	2	1.22
1	1.12	0.89	None	1	1.12	0.89	None	1	1.12
Z	1.12	–	None	Z	1.12	–	None	Z	1.12

Table 12. Group 4 soft storey irregularity controls (continued).

Storey No.	B450C			B500C			B550C		
	η_{ki}(+)	η_{ki}(-)	Control	η_{ki}(+)	η_{ki}(-)	Control	η_{ki}(+)	η_{ki}(-)	Control
5	–	0.48	None	5	–	0.48	None	5	–
4	2.07	0.70	Yes	4	2.07	0.70	Yes	4	2.07
3	1.42	0.81	None	3	1.42	0.81	None	3	1.42
2	1.23	0.88	None	2	1.23	0.88	None	2	1.23
1	1.13	0.39	None	1	1.13	0.39	None	1	1.13
Z	2.59	–	Yes	Z	2.59	–	Yes	Z	2.59

3.2. Weak storey irregularity controls

In the analysis, the same data set was utilized to calculate both soft storey and weak storey irregularities. It's important to note, however, that according to the TBEC-2018 guidelines, ground storey heights are not considered when assessing weak storey irregularity. Instead, the evaluation focuses exclusively on the effective shear areas of the structural elements involved. This distinction highlights the different parameters that influence soft and weak storey irregularities in building design.

In this context, the benefits associated with the use of composite columns in ground storeys become particularly evident. The effective shearing area increases with the incorporation of composite columns due to the addition of structural steel profiles, which enhance the overall strength and stability of the building. As a result, the analytical models can be thoroughly examined based on whether the ground storey columns are made of reinforced concrete or composite materials, allowing for a clearer comparison of their respective performances.

The analysis revealed a noteworthy increase in the strength irregularity coefficient, calculated using Equation 1, when the ground storey columns were designed as composite. Specifically, this coefficient increased by approximately 29% when compared to models utilizing reinforced concrete columns. This substantial change caused the strength irregularity coefficient to rise from 0.66 to 0.85, ultimately surpassing the critical limit of 0.80 established by TBEC-2018. Such an increase in the coefficient indicates a significant shift in the structural behavior, suggesting that composite columns not only enhance the effective shearing area but also improve the overall load-carrying capacity of the ground storey.

The results of this analysis are comprehensively displayed in Table 13, which provides detailed numerical data and comparisons between the various models. This table serves as a valuable resource for understanding the implications of using composite columns in terms of both soft storey and weak storey irregularities.

Overall, these findings emphasize the importance of material choice in structural design, particularly in the context of enhancing shear capacity and addressing irregularities. The increase in the strength irregularity coefficient with the use of composite columns indicates that careful consideration of material properties and structural configurations can lead to improved resilience against lateral forces, such as those encountered during seismic events. This insight is crucial for informing best practices and design strategies in the field of civil engineering, particularly for buildings in areas susceptible to seismic activity.

Table 13. (a) Controls for weak storey irregularity in models with ground storey reinforced concrete columns; (b) Weak storey irregularity in models with composite columns in the ground storey.

Storey No.	Storey height (cm)	η_{ci}		Control	
		(a)	(b)	(a)	(b)
5	300	1.00	1.00	None	None
4	300	1.00	1.00	None	None
3	300	1.00	1.00	None	None
2	300	1.00	1.00	None	None
1	300	1.00	1.00	None	None
Z	Variable	0.66	0.85	Critical*	None

*For $0.60 \leq \eta_{ci} \leq 0.80$, the Structural System Behavior Coefficient given in Table 13, should be multiplied by the value of $1.25(\eta_{ci})$min and applied to the entire building in both earthquake directions.

3.3. Ground storey displacements

As the height of the ground floor increases, the observed displacements in both reinforced concrete and composite column models also rise significantly. This phenomenon can be attributed to the fact that greater heights lead to increased flexibility within the structure, resulting in larger displacements under lateral loads, such as those imposed by wind or seismic activity.

When comparing the two types of models, it is evident that reinforced concrete structures experience more displacement than those utilizing composite columns. This distinction suggests that composite columns enhance the overall rigidity of the structure, thereby effectively mitigating displacement. The differences in ground floor displacement become increasingly pronounced as the height of the ground floor rises. For instance, at a height of 300 cm, the displacement difference between the two models is measured at 0.97 cm. However, this disparity grows substantially as the height increases to 550 cm, where the difference reaches 3.88 cm (Table 14).

This growing divergence emphasizes the enhanced performance of composite columns in taller structures. The ability of composite columns to maintain lower displacement levels becomes increasingly critical as the structure's height increases, making them an effective solution for minimizing displacement in high-rise buildings. This characteristic is particularly advantageous in seismic zones, where excessive displacement can lead to structural failure or significant damage. Furthermore, the findings underscore the importance of considering column material selection when designing taller structures. The flexibility associated with increased height necessitates robust design strategies to ensure structural integrity and safety. Composite columns, with their superior rigidity and lower displacement characteris-

tics, provide a viable alternative to traditional reinforced concrete columns, especially in applications where minimizing lateral movement is paramount.

In summary, the relationship between ground floor height and displacement highlights the significant role that column materials play in structural performance. As building heights continue to increase, the use of composite columns emerges as a preferred choice for engineers seeking to optimize structural rigidity and minimize displacement, thereby enhancing the overall safety and performance of tall buildings. This insight not only informs current design practices but also suggests pathways for future research and development in the field of civil engineering.

Table 14. Reduced ground storey displacements.

Ground storey height (cm)	Ground storey displacements (cm)		Difference in ground storey displacement (cm)
	Reinforced concrete models	Composite column models	
300	5.76	4.79	0.97
350	8.82	7.38	1.44
400	12.64	10.64	2.00
450	17.21	14.60	2.61
500	22.50	19.26	3.24
550	28.47	24.59	3.88

Fig.5 indicates that as the height of the ground floor increases, the structures become more flexible, which reduces the effectiveness of relative floor drift reduction. Buildings with shorter ground floors have a greater advantage in minimizing drift during earthquakes and exhibit higher reduction rates. In contrast, taller ground floors experience larger drifts, making drift reduction measures less effective.

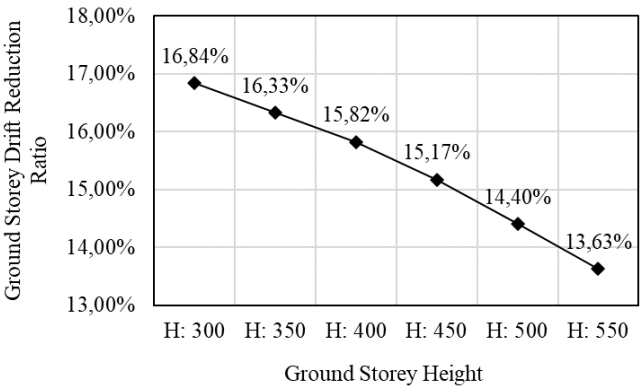

Fig. 5. The use of composite columns decreases the displacement rates of the ground floor.

4. Conclusions

This study looks at how adding wall rigidity impacts soft and weak storey irregularities in buildings without infill walls on the ground storey, and whether composite columns can help fix these problems. It finds that composite columns reduce stiffness differences and ground storey displacements, though longer columns lead to more displacements. Overall, using composite columns is a practical solution to prevent ground or soft storey collapses during earthquakes.

Although TBEC-2018 Information Annex 3A advises avoiding weak and soft storey configurations as much as possible, Section 3.6.2.1 states that A1 and B2 type irregularities only influence the choice of earthquake calculation method according to Section 4.6. As a result, soft storey irregularities are not considered in dynamic analyses. However, as demonstrated in the calculations, including the lateral drift rigidity of infill walls in mathematical calculations even using approximate methods significantly alters the results for soft storey irregularity. Therefore, earthquake codes should include procedures for incorporating wall rigidities into soft storey irregularity assessments. Composite columns in ground storeys can help prevent soft and weak storey issues in structures where infill walls are not used in the ground storey but are present in the upper storeys.

Finally, the impact of using composite columns solely in the ground storey on the selection of the building behavior coefficient and how this should be specifically addressed requires separate examination.

Acknowledgements

None declared.

Funding

The authors received no financial support for the research, authorship, and/or publication of this manuscript.

Conflict of Interest

The authors declared no potential conflicts of interest with respect to the research, authorship, and/or publication of this manuscript.

Author Contributions

All of the authors made substantial contributions to conception and design, or acquisition of data, or analysis and interpretation of data; were involved in drafting the manuscript or revising it critically for important intellectual content; and gave final approval of the version to be published.

Data Availability

The datasets created and/or analyzed during the current study are not publicly available, but are available from the corresponding author upon reasonable request.

REFERENCES

ASCE/SEI 41-17 (2017). Seismic evaluation and retrofit of existing buildings. American Society of Civil Engineers.

Beigi HA, Sullivan TJ, Christopoulos C, Calvi GM (2015). Factors influencing the repair costs of soft-storey RC frame buildings and implications for their seismic retrofit. *Engineering Structures*, 101, 233–245.

Çelik Yapıların Tasarım, Hesap ve Yapım Esaslarına Dair Yönetmelik (2016). Eki: Çelik Yapıların Tasarım, Hesap ve Yapımına Dair Esaslar. Ministry of Environment and Urbanization, Republic of Türkiye, Ankara. (in Turkish)

CSiCol, Design of Reinforced Concrete Columns, v.10, Computers & Structures Incorporated, New York, America.

Elkady A, Lignos DG (2017). Full-scale testing of deep wide-flange steel columns under multi axis cyclic loading: loading sequence, boundary effects, and lateral stability bracing force demands. *Journal of Structural Engineering*, 144(2), 04017189.

Elkady A, Lignos DG (2018). Improved seismic design and nonlinear modeling recommendations for wide-flange steel columns. *Journal of Structural Engineering*, 144 (9), 04018162.

Fakhouri MY, Igarashi A (2013). Multiple-slider surfaces bearing for seismic retrofitting of frame structures with soft first stories. *Earthquake Engineering Structural Dynamics,* 42(1), 145–161.

Hashemi M, Tsang H, Al-Ogaidi Y, Wilson J, Al-Mahaidi R (2017a). Collapse assessment of reinforced concrete building columns through multi-axis hybrid simulation. *American Concrete Instute Structural Journal,* 114(2), 437–449.

Hashemi MJ, Al-Ogaidi Y, Al-Mahaidi R, Kalfat R, Tsang HH, Wilson JL (2017b). Application of hybrid simulation for collapse assessment of post-earthquake CFRP-repaired RC columns. *Journal of Structural Engineering*, 143(1), 04016149.

Hessabi RM, Mercan O (2016). Investigations of the application of gyro-mass dampers with various types of supplemental dampers for vibration control of building structures. *Engineering Structures,* 126, 174–186.

ideCAD, AEC Software for Architecture, Structural Engineering, Structural Detailing, and Construction from Architectural Design to Fabrication, v.10.20, ideYAPI, İstanbul, Türkiye.

Lima C, De Stefano G, Martinelli E (2014). Seismic Response of Masonry Infilled RC Frames: Practice-oriented models and open issues. *Earthquakes and Structures*, 6, 409-436.

Meli R (1986). Evaluation of performance of concrete buildings damaged by the September 19, 1985 Mexico Earthquake. *Proceedings American Society of Civil Engineers International Conference*: *The Mexico Earthquakes 1985. Factors involved and lessons learned*, Mexico City, Mexico, 308-327.

Sahoo DR, Rai DC (2013). Design and evaluation of seismic strengthening techniques for reinforced concrete frames with soft ground storey. *Engineering Structures,* 56, 1933–1944.

Sakino K, Nakahara H, Morino S, Nishiyama I (2004). Behavior of centrally loaded concrete-filled steel-tube short columns. *Journal of Structural Engineering,* 130(2), 180–188.

Shahsahebi A, Waezi Z, Hashemi MJ (2020). Seismic performance assessment of multistorey RC buildings with soft-storey collapse mechanism equipped with gapped inclined bracing (GIB). *Structures*, 28, 2448–2466.

Solak K, Orhan S (2023). Axial compression behaviour of concrete-filled auxetic tubular short columns. *Challenge Journal of Concrete Research Letters*, 14(1), 1-9.

Şermet F, Ercan E, Hökelekli E, Demir A, Arısoy B (2021). The behavior of concrete-encased steel composite column beam joints under cyclic loading. *The Structural Design of Tall and Special Buildings,* 30(6), 1-20.

TBEC (2018). Specifications for buildings to be built in seismic zones (TBDY-2018). Ministry of Environment and Urbanization, Republic of Türkiye, Ankara. (in Turkish)

Tezcan S, Yazıcı A, Özdemir Z, Erkal A (2007). Zayıf kat – yumuşak kat düzensizliği. *Altıncı Ulusal Deprem Mühendisliği Konferansı*, İstanbul, Türkiye, 339-349. (in Turkish)

Ulukaya S, Yüzer N (2017). Tarihi Yapılarda taşıyıcı tuğla duvarın elastisite modülünün deneysel ve matematiksel model ile belirlenmesi. *Uluslararası Katılımlı 6. Tarihi Yapıların Korunması ve Güçlendirilmesi Sempozyumu*, İstanbul, Türkiye, 533-542. (in Turkish)

Van Earthquake Report (2011a). 23 Ekim 2011 mw 7.2 Van depremi sismik ve yapısal hasara ilişkin saha gözlemleri. Report no: METU/EERC 2011-04, Earthquake Engineering Research Center, Middle East Technical University. (in Turkish)

Van Earthquake Report (2011b), 23 Ekim ve 9 Kasım 2011 tarihli Van depremleri yerinde yapılan inceleme ve değerlendirme raporu. İstanbul Kültür University. (in Turkish)

Watanabe F (1997). Behavior of reinforced concrete buildings during the Hyougoken-Nanbu Earthquake. *Cement Concrete Composite*, 19, 203–211.

Yazdi HA, Hashemi MJ, Al-Mahaidi R, Gad E (2021). Multi-axis testing of concrete-filled steel tube columns forming ductile soft-storey in multi-storey buildings. *Journal of Constructional Steel Research,* 183, 106736.

Zengin B (2021). Evaluation of the period and soft story conditions of reinforced concrete buildings with and without infill walls. *Challenge Journal of Structural Mechanics*, 7(3), 151-161.

Zhang Z, Xu P, Gao D, Zhu Y, Nie Y (2018). The study of the seismic performance of the strong-beam and weak-column shaped joints of concrete-filled steel tubular column and steel beams. *3rd International Conference on Smart City and Systems Engineering (ICSCSE)*, Xiamen, China, 413-418.

Challenge Journal of Structural Mechanics

Research Article

Utilization of expired cement and aged roof tile powder in the production of sustainable geopolymer: Mechanical and physical properties

Serdal Ünal [a], Mehmet Canbaz [a,*]

[a] *Department of Civil Engineering, Eskişehir Osmangazi University, 26480 Eskişehir, Türkiye*

ABSTRACT

This study deals with the production of geopolymer mortar in order to promote the recycling of waste materials as sustainable building materials. The use of waste materials such as expired cement and aged roof tiles powders in cementitious systems is of great importance in terms of increasing environmental sustainability and reducing industrial waste. Recycling these materials and using them as alternative binders contributes to more environmentally friendly and economical concrete and mortar production by reducing natural resource consumption. Expired cement and aged roof tile powder were used as binder materials and mortar specimens were produced by activating these materials with alkalis such as NaOH and Na_2SiO_3 at different ratios. Within the scope of the experimental studies, mechanical and physical properties such as unit weight, ultrasonic pulse velocity, compressive strength and bending strength were investigated in detail. The results showed that the expired cement specimens performed better especially in unit weight, ultrasonic pulse velocity and compressive strength tests, while the roof tile powder had superior properties in terms of bending strength. It was also found that the specimens activated with sodium hydroxide (NaOH) exhibited generally higher strength and performance than those activated with sodium silicate (Na_2SiO_3). These findings prove that waste materials such as both expired cement and roof tile powder can be valuable alternatives in the construction industry in terms of sustainability and waste management and reveal the potential of using these materials in geopolymer mortar production.

ARTICLE INFO

Article history:
Received – January 17, 2025
Revision requested – February 14, 2025
Revision received – February 28, 2025
Accepted – March 3, 2025

Keywords:
Geopolymer
Expired cement
Aged roof tile powder
Alkali activation

Citation: Ünal S, Canbaz M (2025). Utilization of expired cement and aged roof tile powder in the production of sustainable geopolymer: Mechanical and physical properties. *Challenge Journal of Structural Mechanics*, 11(2), 82–88.

1. Introduction

Today, rapid urbanisation and industrialisation are increasing the consumption of natural resources and leading to the generation of large amounts of waste. The rapid expansion of the construction sector driven by population growth has presented humankind with unprecedented challenges, primarily due to the significant increase in waste production (Bulut 2024; Şamdan et al. 2024; Shaheen et al. 2024). The recycling and reuse of waste materials is of great importance, both in terms of reducing pollution and conserving natural resources. This approach also plays a crucial role in the building materials industry for a sustainable future (Marrucci et al. 2025). Carbon emissions and energy consumption caused by cement production are among the most important issues in terms of environmental sustainability (Wuyts et al. 2025). The release of greenhouse gases, such as carbon dioxide, contributes to global warming–a major environmental issue that exacerbates disposal problems (Güney and Yıldızel 2024). Therefore, the use of waste materials as alternative building materials sup-

* *Corresponding author*. Tel.: +90-222-239-3750 ; E-mail address: mcanbaz@ogu.edu.tr (M. Canbaz)
ISSN: 2149-8024 / DOI: https://doi.org/10.20528/cjsmec.2025.02.002

Nomenclature

σ_b	Bending strength
σ_c	Compressive strength
A	Area
b	Length
h	Height
l	Distance between supports
M	Mass
P	Load
UPV	Ultrasonic pulse velocity
UW	Unit weight
V	Volume

ports the goals of the circular economy by providing both environmental and economic benefits (Farshadfar et al. 2025). In addition, the use of waste components in building materials not only reduces environmental impact, but also supports economic sustainability by reducing material costs (Menegaki and Damigos 2018). Cement production in particular is a significant contributor to global greenhouse gas emissions due to high energy consumption and carbon emissions, and the use of alternative binding materials has the potential to minimize these negative impacts (Kajaste and Hurme 2016). In addition, the integration of waste materials into the construction sector promotes the use of industrial waste by providing innovative solutions to waste management problems (Ghaffar et al. 2020). Recent studies show that geopolymers and other alternative binder systems have a lower carbon footprint compared to conventional cement and provide adequate strength properties (Neupane 2022; Singh and Middendorf 2020). Such innovative approaches are becoming increasingly important in both academic research and industrial applications in the development of sustainable building materials.

Geopolymer mortars and concretes have become an important area of research in recent years as environmentally friendly and sustainable building materials. Developed as an alternative to traditional Portland cement, these materials have the potential to reduce natural resource consumption and carbon footprint (Chen et al. 2025). Geopolymer materials consist of silica and aluminium containing materials activated by alkaline activators and are characterised by high mechanical strength, low water permeability and chemical resistance. These properties enable geopolymers to find a wide range of applications in the construction industry (Bulińska et al. 2025). However, the type of binders and activation methods used in the production of geopolymers play a critical role in the performance of the final product (Milad 2025). Geopolymer mortar is a sustainable alternative to conventional cement, offering durability and resistance to chemical attack. It has practical applications in infrastructure rehabilitation, precast elements, fire-resistant coatings, and 3D printing. However, challenges related to scalability, long-term performance, and standardization must be addressed for widespread adoption. Future research in this area will focus on optimising production methods, improving durability and developing regulatory frameworks for successful implementation.

This study investigated the potential of using expired cement and aged roof tile powder as binders in the production of geopolymer mortars. Specimens of expired cement and aged roof tile are shown in Fig. 1. The mechanical and physical properties of mortar specimens activated with alkalis such as NaOH and Na_2SiO_3 at different ratios were tested. The originality of this study stems from its comprehensive evaluation of the potential of using expired cement and aged tile powder as alternative binders in geopolymer mortar production. While materials such as fly ash, blast-furnace slag, and metakaolin have generally been investigated as geopolymer binders in the literature, this study analyzed in detail the effect of recyclable materials such as waste cement and tile powder on geopolymer performance. In this respect, the research provides a new perspective in the field of sustainable building materials. As a result of the experimental studies, it was observed that the use of old cement and tile powder significantly affected the strength properties of geopolymer mortars. Our study contributes to the use of more sustainable materials in the construction industry by revealing the recycling potential of waste materials such as expired cement and tile powder. In particular, the improvement in performance of the NaOH activated specimens highlights the effectiveness of this method. The results obtained are an important step towards the sustainable use of waste materials in the construction sector.

Fig. 1. Expired cement and aged roof tile.

2. Experimental study

2.1. Materials

In this study, expired cement and aged roof tile powder were used as binders and Na_2SiO_3 and NaOH solutions were used as alkali activators in the production of geopolymer mortars. The chemical properties of the materials used are given below.

- Binder: Expired cement and tile powder were used as binders in the study. CEM I 42.5R cement produced by ÇİMSA (Eskişehir, Türkiye) was used. The mechanical, physical and chemical properties of the cement used are shown in Table 1, while the properties of the waste tiles used in the experiment are given in Table 2.
- Water: Eskişehir city mains water was used in mortar production. The chemical analysis of the water used is given in Table 3.
- Alkalis: NaOH and Na_2SiO_3 were used to activate the waste materials. The chemical properties of the materials used are given in Tables 4 and 5.

Table 1. Properties of cement.

Cement (CEM I 42.5 R)	Specific gravity	Fineness (cm^2/g)	CaO	SiO_2	Al_2O_3	Fe_2O_3	SO_3	Na_2O	K_2O	MgO
			(%)							
	3.11	0-3	63.62	19.23	5.44	3.48	2.17	0.68	0.55	0.88

Table 2. Properties of aged roof tile.

Specific gravity	Density (kg/m^3)	Water absorption (wt%)	Abrasion (Los Angeles) (%)
0.925	1904	11.56	82

Table 3. Properties of water.

Water	pH	SO_4	Ca	Mg	Cl	Na	K
		(kg/dm^3)					
	7.27	45	21.10	12.20	9.82	8.30	3.00

Table 4. Properties of NaOH.

NaOH	Na_2CO_3	NaCI	Fe
≥98.0	≤0.4	≤0.05	≤0.001

Table 5. Properties of Na_2SiO_3.

Na_2O	SiO_2	Density (kg/dm^3)	Module
8.57	26.73	1.316	2.87

2.2. Method and tests

In the production phase, the materials that we have defined as waste (expired cement and roof tile powder) were ground in the shaft mill as the first step. After the grinding process was completed, the materials were sieved through a 150 micron sieve. In the production of geopolymer mortars, mortars were produced with only NaOH as alkali activator, with NaOH/Na_2SiO_3 solution in the ratio of 1:2, and with only Na_2SiO_3. During the production phase, a 12 M NaOH solution was prepared approximately 26 hours in advance. As the dissolution of NaOH in water is a highly exothermic reaction that releases significant heat, the solution was left to cool to ambient temperature for about 2 hours (İpek and Ekmen 2022). Consequently, the NaOH solution was prepared approximately 2 hours prior to mixing with the Na_2SiO_3 solution. The alkali activator solution was then prepared by combining predetermined amounts of NaOH and Na_2SiO_3 solutions approximately 24 hours before being utilized in the production of geopolymer mortar. The production process began by mixing the binders with the alkali activator solution in a mixing pan for 3 minutes to produce geopolymer paste. Once the paste was formed, sand was gradually added to the mixer, and the mixture was stirred for an additional 3 minutes to complete the mixing process. A flowchart illustrating the entire production sequence, from the initial preparation of the NaOH solution to the completion of the manufacturing process, is shown in Fig. 2.

Mortar specimens produced were tested for unit weight, ultrasonic pulse velocity, bending and compressive strength. Ultrasonic pulse test was used to determine the effect of placement and structural voids that may occur in the geopolymer specimen, unit weight was calculated since weight is important in applications, compression and bending test methods were used to determine the mechanical properties. Unit weight was calculated using equation $UW=M/V$, ultrasonic pulse velocity using equation $UPV=L/T$, compressive strength using equation $\sigma_c=P/A$ and bending strength using equation $\sigma_b=1.5\cdot(Pl)/(bh^2)$. Fig. 3 shows the equipment and tools used in the experiments.

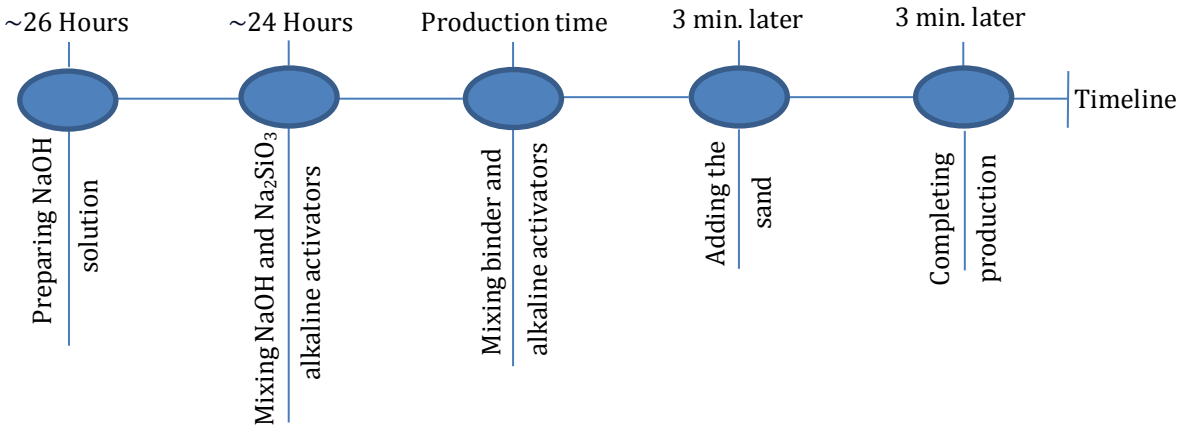

Fig. 2. Timeline of geopolymer mortar production.

Fig. 3. Test equipment to determine physical and mechanical properties.

3. Results and Discussion

3.1. Unit weight analysis

Fig. 4 shows the unit weight analysis results of the specimens containing expired cement and aged roof tile powder binders with different alkali activators. When analysing Fig. 4, it can be seen that the mortar specimens with expired cement binder have higher unit weight values than the specimens with aged roof tile powder binder. This can be explained by the fact that the unit weight of cement is higher than the unit weight of roof tile powder. While the highest density of 1.8 g/cm^3 was obtained from the specimens with expired cement binder, the highest density of 1.52 g/cm^3 was obtained from the specimens with roof tile powder. This may also indicate that there are fewer micro voids in the structures of the specimens with expired cement. When analysed according to the content of alkali activators, mortar specimens containing only Na_2SiO_3 achieved the highest unit weight value in both binder types. In the specimens containing old cement, the unit weight of the specimens containing Na_2SiO_3 was 10% higher than that of the specimens containing NaOH. In the mortar specimens with aged roof tile powder binder, the unit weight of the specimens containing Na_2SiO_3 was 9% higher than the specimens containing NaOH.

3.2. Ultrasonic pulse velocity analysis

Fig. 5 shows the results of the ultrasonic pulse velocity analysis of the specimens containing expired cement and aged roof tile powder binders with different alkali activators. When analysing Fig. 5, the highest ultrasonic pulse velocity of 4.47 km/sec was obtained in the specimens with expired cement binder, while the highest ultrasonic pulse velocity value of 3.73 km/sec was obtained in the aged roof tile powder specimens. It was found that the mortar specimens with expired cement binder had higher ultrasonic pulse velocity values than the aged roof tile powder binder specimens. The expired cement geopolymer mortar specimens have higher unit weight values compared to the aged roof tile powder binder mortars and therefore have fewer voids in their structure. A lower void ratio results in a high ultrasonic pulse velocity. When the alkali activators were analysed according to their content, mortar specimens containing only Na_2SiO_3 reached the highest value of the ultrasonic pulse velocity in both binder types. In the specimens containing expired cement, the unit weight of the specimens containing Na_2SiO_3 was 13% higher than that of the specimens containing NaOH. In the mortar specimens with tile powder binder, the unit weight of the specimens containing Na_2SiO_3 was 14% higher than the specimens containing NaOH.

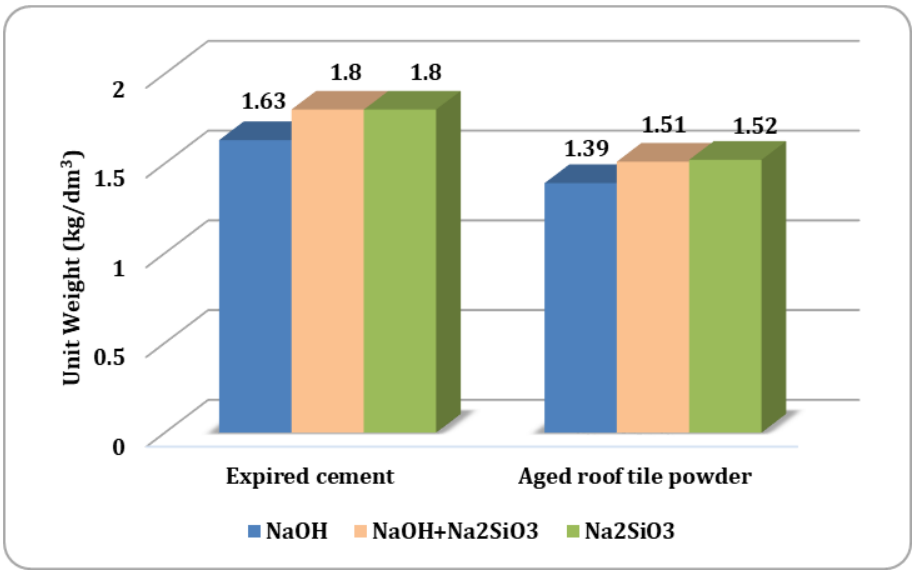

Fig. 4. Unit weight analysis results of the specimens.

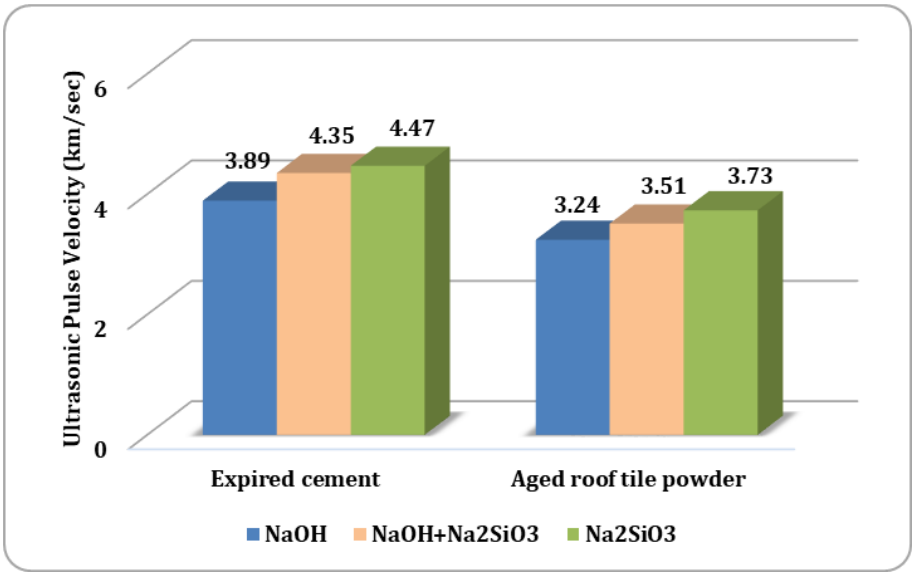

Fig. 5. Ultrasonic pulse velocity analysis result of the specimens.

3.3. Bending strength test

Fig. 6 shows the bending strength test results of the geopolymer mortar specimens. It can be clearly seen from Fig. 6 that the use of expired cement as a binder gives higher bending strength results than the use of tile powder. Similar results have been obtained in the literature depending on the material ratio and production method (Naenudon et al. 2022). The use of Na_2SiO_3 as an alkali activator in expired cement gave 8% higher bending strength results than the use of NaOH. In geopolymer mortar specimens using tile powder as a binder, the use of Na_2SiO_3 resulted in 9% higher bending strength than the use of NaOH.

3.4. Compressive strength test

Fig. 7 shows the compressive strength test results of the geopolymer mortar specimens. In Fig. 7, as with the bending strength results, it is clearly seen that the use of expired cement as a binder result in higher compressive strengths than the use of roof tile powder. Similar results have been obtained in the literature depending on the material ratio and production method (Mahmoodi et al. 2020, 2021; Usha et al. 2016).

It can be seen that the higher unit weight and filling ratio in the expired cement specimens have a direct effect on the higher compressive strength results. The highest compressive strength value of 18.78 was obtained from the expired cement specimens, while the highest compressive strength value of 14.77 was obtained from the aged roof tile powder specimens. When Na_2SiO_3 was used as an alkali activator in expired cement, the compressive strength results were 9% higher than NaOH. In geopolymer mortar specimens using aged roof tile powder as a binder, the compressive strength was 4% higher when Na_2SiO_3 was used than when NaOH was used.

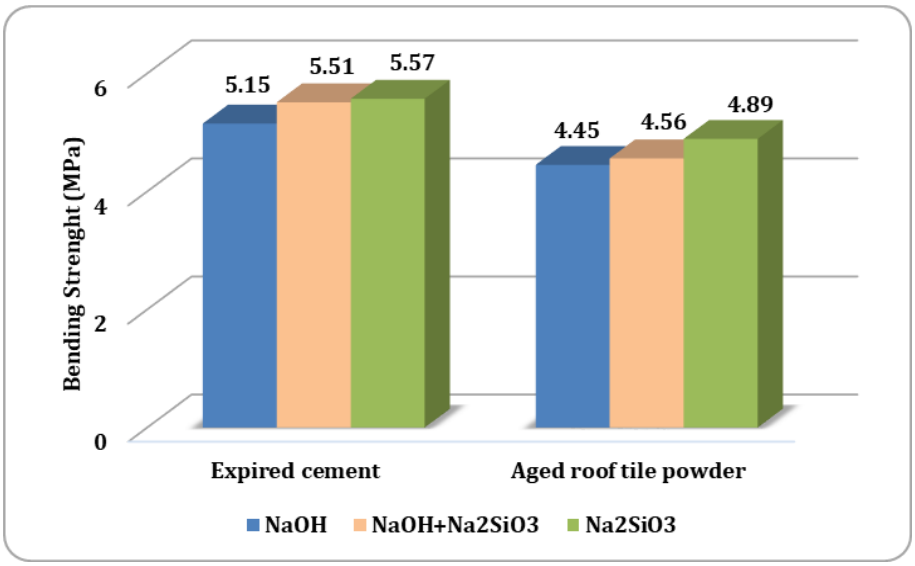

Fig. 6. Bending strength test results of the specimens.

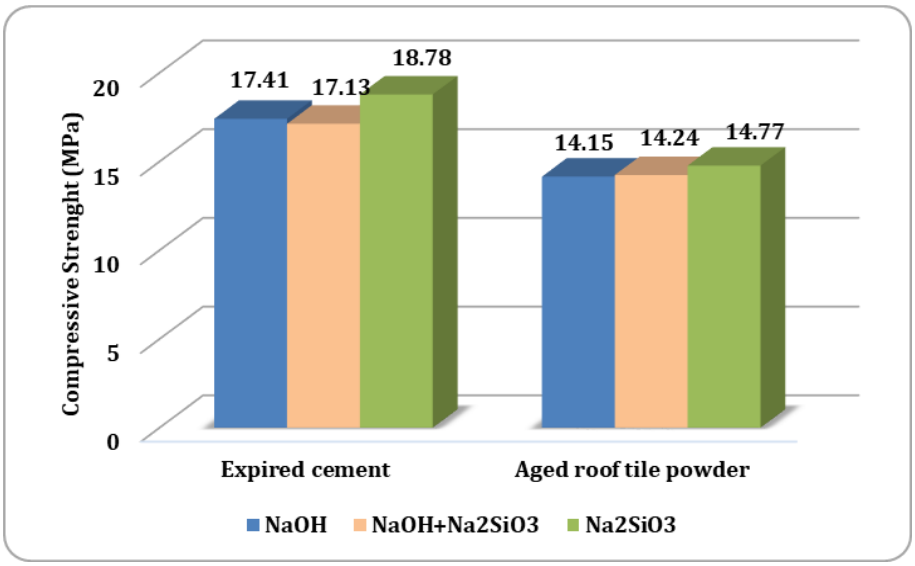

Fig. 7. Compressive strength test results of the specimens.

Recycling expired cement and aged roof tile powder into construction products as geopolymers offers significant environmental and economic benefits. This process reduces natural resource consumption by up to 30% by utilizing waste materials, while increasing environmental sustainability by reducing carbon emissions by up to 60% and energy consumption by 50% compared to cement production. In addition, it provides cost savings of up to 25% in the construction sector with its low raw material cost, while the up to 50% longer life of geopolymer-based building elements reduces maintenance and repair costs. The development of geopolymer technology with such waste materials offers a sustainable alternative in both environmental and economic terms.

4. Conclusions

As a result of the tests and analyses performed on geopolymer mortars containing waste binder, the following results were obtained:

- The geopolymers produced using expired cement had significantly higher unit weight and ultrasonic pulse velocity values compared to the specimens using aged roof tiles powder as a binder. Unit weight of 1.8 g/cm^3 and an ultrasonic pulse velocity of 4.47 km/sec have been obtained. These results are particularly important for the use of expired cement in the production of sustainable materials.
- Geopolymers produced using expired cement had significantly higher compressive and bending strength values compared to the specimens using aged roof tiles powder as binder. 18.78 MPa compressive strength value and 5.57 MPa bending strength were obtained. These results showed that geopolymer with high compressive and bending strength can be produced with waste materials.
- The use of Na_2SiO_3 alone as an alkaline activator showed better results in all experiments than the use of NaOH-Na_2SiO_3 and NaOH alone. In general, it was found that high mechanical and physical properties were obtained with the use of these activators.

In this study, it is shown that expired cement and aged roof tile powder can be used effectively in geopolymer mortar production. While it is recommended to use Na_2SiO_3 as an alkali activator, it can be used with waste binder to provide the required mechanical and physical properties. For future studies, it is recommended to investigate the effect of different curing conditions on these materials, develop hybrid binder systems with different waste materials and investigate their long-term durability performance. Thus, more efficient use of recycled binders in geopolymer systems can be achieved.

Acknowledgements

None declared.

Funding

The authors received no financial support for the research, authorship, and/or publication of this manuscript.

Conflict of Interest

The authors declared no potential conflicts of interest with respect to the research, authorship, and/or publication of this manuscript.

Author Contributions

All of the authors made substantial contributions to conception and design, or acquisition of data, or analysis and interpretation of data; were involved in drafting the manuscript or revising it critically for important intellectual content; and gave final approval of the version to be published.

Data Availability

The datasets created and/or analyzed during the current study are not publicly available, but are available from the corresponding author upon reasonable request.

REFERENCES

Bulińska S, Sujak A, Pyzalski M (2025). Sustainable management of photovoltaic waste through recycling and material use in the construction industry. *Materials*, 18(2), 284.

Bulut HA (2024). A different approach for green concrete production: Determination of the effect of e-waste and waste rubber powder on durability properties of concrete. *Challenge Journal of Concrete Research Letters*, 15(3), 69-81.

Chen Y, Zou C, Yeo JS, Lin J, Tan TH, Mo KH (2025). Valorization of high-volume crushed waste glass as fine aggregate in foamed geopolymer. *Case Studies in Construction Materials*, e04202.

Farshadfar Z, Khajavi SH, Mucha T, Tanskanen K (2025). Machine learning-based automated waste sorting in the construction industry: A comparative competitiveness case study. *Waste Management*, 194, 77-87.

İpek S, Ekmen Ş (2022). Investigation of recycling of building materials as sand ın the production of geopolymer mortar. *Adıyaman University Journal of Engineering Sciences*, 9(17), 404-419.

Ghaffar SH, Burman M, Braimah N (2020). Pathways to circular construction: An integrated management of construction and demolition waste for resource recovery. *Journal of Cleaner Production*, 244, 118710.

Güney B, Yıldızel S (2024). Optimization of mechanical properties in lime-based composites using the Taguchi method. *Challenge Journal of Structural Mechanics*, 10(3), 109-115.

Kajaste R, Hurme M (2016). Cement industry greenhouse gas emissions–management options and abatement cost. *Journal of Cleaner Production*, 112, 4041-4052.

Mahmoodi O, Siad H, Lachemi M, Dadsetan S, Sahmaran M (2020). Development of ceramic tile waste geopolymer binders based on pre-targeted chemical ratios and ambient curing. *Construction and Building Materials*, 258, 120297.

Mahmoodi O, Siad H, Lachemi M, Dadsetan S, Sahmaran M. (2021). Development of optimized binary ceramic tile and concrete wastes geopolymer binders for in-situ applications. *Journal of Building Engineering*, 43, 102906.

Marrucci L, Daddi T, Iraldo F (2025). Boosting circular economy solutions in the construction sector using a life cycle assessment. *Journal of Industrial Ecology*, 29(2), 473-485.

Menegaki M, Damigos D (2018). A review on current situation and challenges of construction and demolition waste management. *Current Opinion in Green and Sustainable Chemistry*, 13, 8-15.

Milad A (2025). Recycled and upcycled materials in contemporary architecture and civil engineering: Their applications, benefits, and challenges. *Cleaner Waste Systems*, 10, 100203.

Naenudon S, Vilaivong A, Zaetang Y, Tangchirapat W, Wongsa A, Sata V, Chindaprasirt P (2022). High flexural strength lightweight fly ash geopolymer mortar containing waste fiber cement. *Case Studies in Construction Materials*, 16, e01121.

Neupane K (2022). Evaluation of environmental sustainability of one-part geopolymer binder concrete. *Cleaner Materials*, 6, 100138.

Shaheen YBI, Etman ZA, Mohamed AAF (2024). Structural behavior of ferrocement beams with circular openings. *Challenge Journal of Structural Mechanics*, 10(4), 116-137.

Singh NB, Middendorf B (2020). Geopolymers as an alternative to Portland cement: An overview. *Construction and Building Materials*, 237, 117455.

Şamdan F, Çelikyürek İ, Canbaz M (2024). Determination of waste crushed baked clay aggregate concrete with granular composite material preparations. *Challenge Journal of Concrete Research Letters*, 15(4), 112-119.

Usha S, Nair DG, Vishnudas S (2016). Feasibility study of geopolymer binder from terracotta roof tile waste. *Procedia Technology*, 25, 186-193.

Wuyts W, Strøm-Andersen N, Khatri S, Eriksen A, Jørgensen PF, Øvergaard A, Nore K (2025). SirkTRE's evolution or circulution?: Diverse pathways of circular systemic solutions for a Net-Zero timber-built environment. In: Kioumarsi, M., Shafei, B. (eds) *The 1st International Conference on Net-Zero Built Environment. NTZR 2024. Lecture Notes in Civil Engineering*, vol 237. Springer, Cham.

Challenge Journal of Structural Mechanics

Research Article

Influence of connector forces on the expansion configuration of a hexagonal modular floating structure

Nur Hanani Ahmad Azlan [a,*], Nik Mohd Ridzuan Shaharuddin [b], Arifah Ali [a]

[a] *Department of Aeronautics, Automotive and Ocean Engineering, Universiti Teknologi Malaysia, 81310 Johor Bahru, Malaysia*
[b] *Marine Technology Centre, Institute for Vehicle System and Engineering, Universiti Teknologi Malaysia, 81310 Johor Bahru, Malaysia*

ABSTRACT

The preliminary design of a hexagonal modular floating structure (HMFS) system includes two configurations: U-shaped and V-shaped, which link seven hexagonal modules that create a network of connectors. The connector force is a crucial consideration in the layout of the connector network, as it must sustain the forces generated by wave motion due to its influence on the stability and safety of the modular floating structure. This paper presents the development of the HMFS connector network and the estimation of the connector horizontal force influence by two types of configurations. The design concepts of these configurations for HMFS configurations are proposed where analysis was implemented for regular wave in various directions of 0°, 30°, 45°, 60°, 85°, and 90°. The impact of these various wave directions and the HMFS configurations on the connector force is analysed accordingly. According to this research finding, the connector force in U-shaped configuration is higher than the load in V-shaped of HMFS configuration. The connector force of the V-shaped configuration is arranged in hexagonal vertices (VV-shaped) facing wave direction receive a higher connector force than hexagonal parallel sides (VP-shaped) facing wave directions. The determination of horizontal connector load of hexagonal modules with varying configurations enabled the designer to estimate the horizontal connector load for various conceptual designs of hexagonal shapes, such as dock ships, yacht terminal and floating cities.

ARTICLE INFO

Article history:
Received – December 13, 2024
Revision requested – January 20, 2025
Revision received – March 14, 2025
Accepted – March 20, 2025

Keywords:
Hexagonal floating structure
Connector force
Connector arrangement
Module arrangement

Citation: Azlan NHA, Shaharuddin NMR, Ali A (2025). Influence of connector forces on the expansion configuration of a hexagonal modular floating structure. *Challenge Journal of Structural Mechanics*, 11(2), 89–98.

1. Introduction

The development and exploitation of the ocean have become significantly more diverse due to the growing human demand and advancements in ocean engineering technology (Song et al. 2023; Park et al. 2023). The design of ocean structure has evolved from traditional ships to complex interconnected platforms for various functions (Song et al. 2023), such as space resources (Wong et al. 2013), ocean energy utilization, etc. A single floating structure with large sizes of floating structure could cause massive loads in structures; thus, the types of modular floating structure are preferred which has advantages for constructure, transportation and deployment (Watanabe et al. 2004). The structure is fabricated in modularized and the modules are assembled with connectors at the operation location owning to the large size of floating structure. Very large floating structures (VLFS) for the purpose of floating islands have been grouped into two: semi-submersible suitable use in open oceans and pontoon types suitable for mild seas (Park et al. 2023). Furthermore, the location of the central module, tail module and outer module in deciding the arrangement of the multi-floating structure gives effect to the motion characteristic of floating islands (Park et al. 2023).

* *Corresponding author*. E-mail address: nhanani4@gmail.com (N. H. A. Azlan)
ISSN: 2149-8024 / DOI: https://doi.org/10.20528/cjsmec.2025.02.003

1.1. Conceptual design of modular floating structure

Six sides of a hexagonal regular polygon give advantages to the researcher in expanding their decision making to arrange the modular floating structure with their creativity and purpose of the floating structure. Xiaozhou et al. (2024) conducted the experiment to investigate the hydrodynamic performance of the double module hexagonal floating structure in a linear arrangement. Three hexagonal modular floating structures arranged in linear and L-shaped arrangements by Ikegami et al. (2007). Vincenzo (2023) studied the behaviour of three hexagonal platforms that were arranged in linear arrangement on the surge, heave and pitch degrees of freedom through simulation for regular and irregular waves. Li et al. (2023) modified the design layout by proposing four hexagonal modules, one in the middle module and another module arranged in an L-shaped attachment to the middle module. Li et al. (2022) also studied the linear arrangement linked to a five modules hexagonal shape floating structure. Li et al. (2024) conducted the experiment to investigate the hydrodynamic performance of five hexagonal floating structures in linear arrangement. Hamamoto and Fujita (2016) investigated the hydrodynamic motion of seven hexagonal modular floating structures introduced in two types of arrangements: are in centralized shaped and stretched shaped as shown in Fig.1.

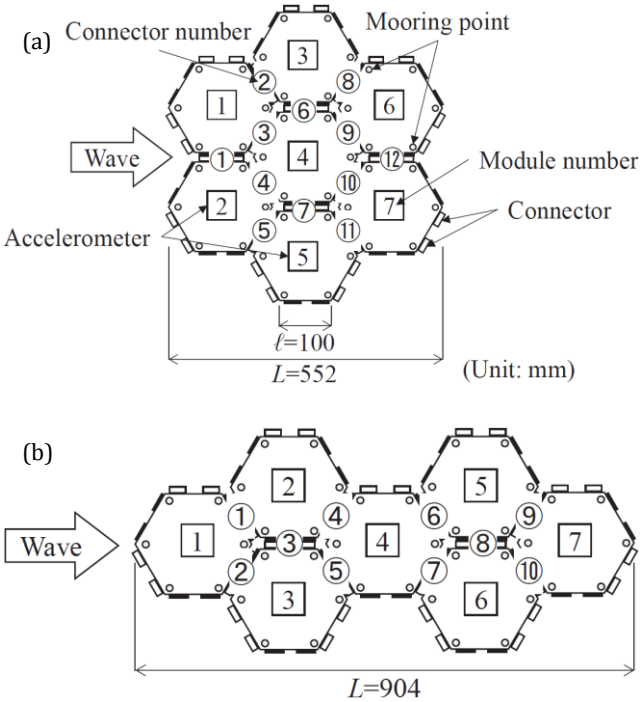

Fig. 1. Two arrangements of hexagonal modular floating structure proposed by Hamamoto and Fujita (2016): (a) Centralized shape; (b) Stretched shape.

Nowadays, the exploration of hexagonal modular floating structures into the development of floating cities gives expansion an additional higher number of modular floating structures rather than a small number floating within two to seven modules linked together. Wong et al. (2013) proposed three arrangement hexagonal modular floating structure comprising 493 modules, 352 modules in one circular pattern to build a man-made island on water bodies for recreational activities and amenities for the public, and a sanctuary for plants, birds and other wildlife for Punggol floating wetlands. Moreover, Lister and Muk-Pavic (2015) described a sustainable artificial island designed for Republic of Kiribati's inhabitants and explore the layout of hexagonal modular floating arranged U-shaped and centralized arrangements. Stanković et al. (2021) proposed the modular floating structure arranged in regular tessellation in triangular, square and hexagonal shapes for Kiribati Island. Jiang et al. (2021a) investigated the hydrodynamic analysis of a hexagonal modular floating structure in a linear tandem arrangement with a size of 251.9×66 m and 137.4×132 m looking as one square shape.

1.2. Internal connector force analysis

The connector system suffers force and bending moment from the adjacent module which is the commonly most fragile component of the whole structure, thus, the interaction between the connector and modules should be studied due to the loading characteristic of the is also key part for the very large multi-floating structure (Li et al. 2022). Dai et al. (2021) compared connection loads of difference design options of the multi-floating floating structure such rectangular, square and hexagon, then the small different in terms of shear force and twisting between rectangular and hexagonal but still the connection bending moment for hexagonal is lower 27% than rectangular. Li et al. (2022) investigated the connector forces which include horizontal force, vertical force, shear force and pitch bending moment at wave directions of 0°, 30°, 60° for five hexagonal modules linked in a linear arrangement. Li et al. (2023) investigated the connector forces includes horizontal force, vertical force, shear force and pitch bending moment at wave directions of 0°, 30°, 60° and 90° for five hexagonal modules linked in the center and an L-shaped concept arrangement. Ikegami et al. (2007) stated the connecting horizontal force in the L-shape arrangement become larger in the longer wave period range as a complex behaviour pattern in L-shaped may occur due to each floating body facing the different direction of incident waves. Xiaozhou et al. (2024) investigated how the relative pitch motion of the two modules affects the connector loads the most such as using a larger cable stiffness, which will reduce the pitch motion, but increase the connector loads.

Jiang et al. (2021b) mentioned that the internal forces generated in the connector significantly affected the structural integrity during wave action. However, only a few of studies have performed numerical evaluations of these internal forces, encompassing module arrangements, shallow water effects and incident wave periods. The trend of the connector load depending on the shape of the floating structure. The horizontal connector force trend of five square modular floating structures, as presented by Riggs et al. (1998), indicated a gradually increase in horizontal connector force from 0° wave direction to 75° wave directions, a sharply decline at 80° wave directions, with the peak horizontal connector force occurring at 85° wave di-

rections. The trend of horizontal connector force has also been similar to the rectangular modular floating structure that has been proposed by Ding et al. (2020), wherein the highest horizontal connector force at 85° wave directions linked three rectangular modular floating structures. Meanwhile, Otto et al. (2019), Hongtao et al. (2020), and Azlan et al. (2024) identified that the higher horizontal connector force for the hexagonal modular floating structure occurs at 0° wave direction. Otto et al. (2019) built the combination of triangular module that has 60° connector directions that create a big hexagonal module, then he asserted that to avoid a typical in-line environment with less than 30° spreading into wind, waves and current as it will give the higher connection loads. Azlan et al. (2024) studied five modules of HMFS together in a linear arrangement and discovered that 0° wave direction gives higher connector force and gradually reduces the horizontal connector force as the wave direction increases.

The objective of this research is to determine the impacts of different wave directions on the maximum horizontal connection load, while varying the HMFS arrangements. The hexagonal shape of the modular floating structure facilitates diverse designs, as its six sides can be arranged without gaps. Therefore, the suitable arrangement should been design in the conceptual design of modular floating structure, taking into account the effects of connector load.

2. Materials and Method

2.1. Conceptual design of hexagonal modular floating structure *(HMFS) system*

The idea configuration of the HMFS system was identified by a literature review. The idea from Stanković et al. (2021) and Lister and Muk-Pavic (2015) was adopted and three configurations of the HMFS system were proposed in this research: such as U-shaped and V-shaped, while V-shaped is divided into two configurations that take into account the sides hexagonal (VP-shaped) and vertices hexagonal (VV-shaped) shown in Fig. 2. These three concepts of HMFS system arrangement are exposed to the conceptual design of floating structures. The VP-shaped arrangement of floating cities proposed by from Stanković et al. (2021) illustrates the layout has been adopted to express communication, especially in terms of transportation between the central module and side circular modules. Meanwhile, the primary functions in floating cities, including governance area, commercial area and hospitality area and water transportation are organized in the U-shaped arrangement of floating cities, ensuring that all facilities are centrally located close to one another. Lister and Muk-Pavic (2015) proposed the residential area presented in the VV-shaped arrangement of floating cities.

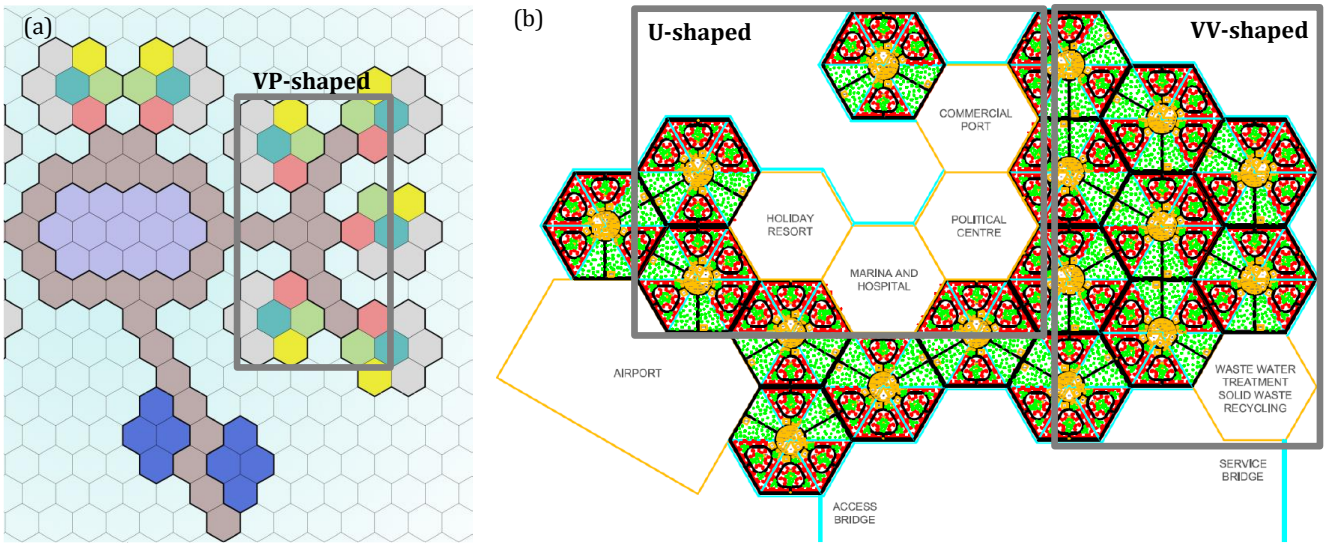

Fig. 2. The idea of HMFS system arrangement for (a) VP –shaped by Stanković et al. (2021); and (b) U- and VV-shaped configurations by Lister and Muk-Pavic (2015).

There are seven hexagonal modules (M1-M7) linked with a ball connector for each configuration of HMFS system as shown in Fig. 3. The main module is the M1 module, which acts as the pivot point of a symmetrical module layout. The overall configuration starts with M1 as the middle, the top continues sequentially with M2, M4 and M6, while the bottom is arranged with M3, M5 and M7. The numbering of connectors also follows the same ideology by continuing sequentially as top (C1, C3, C5) and bottom (C2, C4, C6) as numbering of hexagonal modules. The U-shaped arrangement presents the central module as M1 as the inner module, while the top modules and bottom module are arranged in linear arrangements and early modules face wave force. The VP-shaped presented the module M1 as the center and early facing the wave force, while both top and bottom modules are arranged in staggered arrangements. The parallel side of the hexagon is facing the 0° wave direction for both the U-shaped and V-shaped of HMFS arrangements. The VV-shaped also arranged the modules M1 as the central, meanwhile implement combination of a linear layout for bottom modules and a staggered layout for top modules. The vertices sides of the hexagon are arranged facing the 0° wave direction.

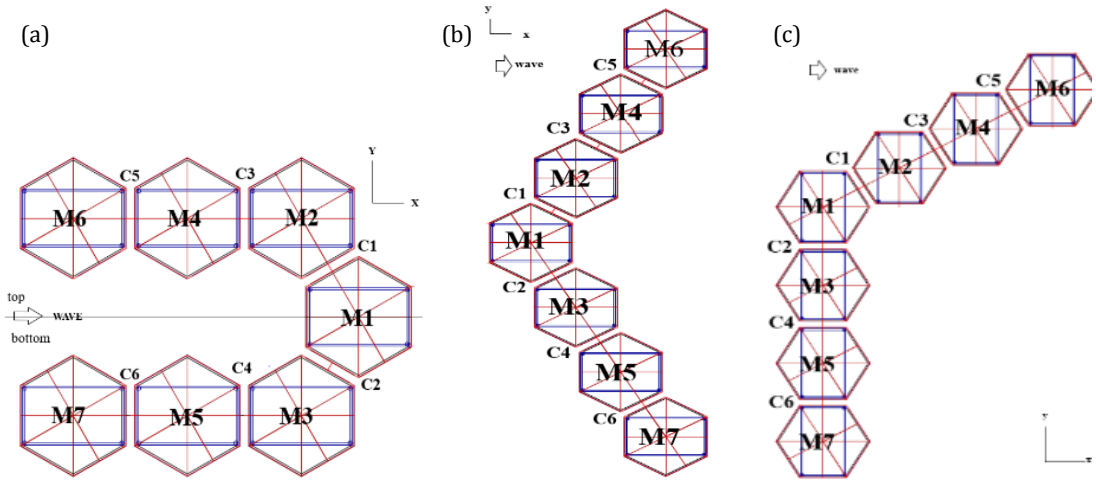

Fig. 3. Three configurations of hexagonal modular floating structure (HMFS): (a) U-shaped; (b) V-shaped, parallel sides facing wave (VP); (c) V-shaped, vertices facing wave (VV).

The detailed design of all components for HMFS, included the hexagonal floating structure, connector and mooring was adopted by Li et al. (2023). Each hexagonal floating structure is linked with a ball connector and moored with four tension legs to the seabed. The fenders have also been installed at the bottom edge of adjacent modules to avoid a possible collision. The details of the HMFS system are shown in Table 1.

Table 1. Details about the HMFS system.

Details	Value	Unit
Side length, height	20, 12	m
Water depth, draft	80, 10	m
Mass	6000	t
$I_{xx} = I_{yy}$	9.6 x10^8	m^4
Tension – leg dimension	D=1.2; T=0.04; L=70	m
Steel tension leg	2.1 x 10^{11}	N/m^2
Stiffness of fenders	1.0 x 10^7	N/m
Adjacent distance	3	m
Ball connector linear rotational dampers	4 x 10^9	Nms/rad
Ball connector linear rotational springs	0	Nms/rad

2.2. Simulation

The maximum horizontal force of each configuration was investigated under a regular sea condition (T=8s, H=2m) with different incident wave direction such as 0°, 30°, 45°, 60°, 85°, 90°). The motion responses of each hexagonal and the maximum horizontal force under different wave direction was simulated using ANSYS. The governing equation of HMFS system in ANSYS (2013) is:

$$M_i\ddot{X}_i + C_i\dot{X}_i + K_i(X_i) = F_{i,wave} + F_{i,con} + F_{i,TLP} + F_{i,Fender} \quad (1)$$

where M_i, C_i and K_i are the mass matrix, radiation damping (with certain artificial damping usually applied to compensate for viscous fluid effects) and the hydrostatic restoring matrix, respectively. Xi (6-DOF) denotes the generalized displacement vector of the i-th module. $F_{i,\text{wave}}$, $F_{i,\text{Con}}$, $F_{i,\text{TLP}}$ and $F_{i,\text{Fender}}$ denote the matrix of the generalized wave force, the connector force, the tension matrix of tension legs and the impact force matrix of fender, respectively. The connector force between adjacent modules can be expressed as:

$$F_{i,con} = \sum_{j=1}^{7} (\varphi_{ij}\, K_{cij}\, \delta(X_i, X_j)) \quad (2)$$

where φ_{ij} denotes a topology matrix. The value of φ_{ij} is 1 when the i-th module is connected to the j-th module, otherwise the value of φ_{ij} is 0. K_{cij} and $\delta(X_i,X_j)$ denote the connection stiffness matrix and the relative motion matrix between the i-th module and the j-th module, respectively. The total tension-leg force of the i-th module can be expressed as:

$$F_{i,TLP} = \sum_{j=1}^{4} E_i\, A_i \varepsilon_{ij} \quad (3)$$

where E_i denotes the elastic modulus. A_i denotes the sectional area of the tension leg of the i-th module. ε_{ij} denotes the strain of the j-th tension leg of the i-th module.

The possible bottom fender impact force $F_{i,\text{fender}}$ can be expressed as:

$$F_{i,fender} = \begin{cases} K_{fij} . \quad \delta x, \text{if } \delta x(X_i, X_i) < -3 \text{ m (contact)} \\ 0 \qquad\qquad \text{if } \delta\, x(X_i, X_i) < -3 \text{ m (contact)} \end{cases} \quad (4)$$

where K_{fij} (1x10^7 N/m) is the bottom fender linear stiffness coefficient between the i-th module and the adjacent j-th module. $\delta x(X_i,X_j)$ is the relative bottom surge motion between the i-th module and the adjacent j-th module. If the negative relative bottom surge motion $\delta x(X_i,X_j)$ is smaller than the module gap (3m), the two adjacent modules will impacts on the bottom. Then, the contact force at the bottom fenders will be monitored.

3. Results and Discussion

There are seven hexagonal modules (M1-M7) linked with a ball connector for the HMFS system, which can create more configurations because the hexagon having six sides. The VP configuration involves connecting a series of HMFS in a vertical, staggered configuration, whereas the VV configuration is more closely resembles an L-shaped configuration. Nowadays, all these configurations are applied in various functions of floating structures, for instance, breakwater, floating solar farm, floating city and etc. Moreover, designers can create many other configurations with hexagonal floating structures, for example in floating city planning, the U-shaped combined with the V-shaped placed the danger function like a power system located further than residential, and the U-shaped used for trade shipping business. This paper only presents linear arrangement but expands in the layout of U-shaped and V-shaped due to limitations in simulation.

Other than linear arrangement, currently some researchers have done the hydrodynamic analysis for centered arrangement that linked seven modules of HMFS by Hamamoto and Fujita (2016). Park et al. (2023) also focus on hydrodynamic analysis of floating structures with expansion of the central module that create a circular hexagonal modular floating structure. Then, Dai et al. (2021) also studied hydrodynamic analysis of floating structure but expansion of HMFS in terms of tandem arrangement that expansion by side by side. Wong et al. (2013) have done simulation that in a centralized arrangement linked many hexagonal modular given a result one maximum shear force that assuming all the connector forces has the same connector force. Besides, nowadays, many research only gives attention to the dynamic analysis for HMFS because it is a new area discovered. The analysis of connector force for each connector of multi-floating should be studied because connectors are also key parts for the stability and safety of modular floating structures.

This paper presents the maximum horizontal connector force in different arrangements which comprises seven modules of HMFS, including U-shaped, VP-shaped and VV-shaped. This is because, Lan et al. (2004) stated that the longitudinal forces are in general substantially larger than the transverse and vertical forces; therefore, the focus is on these forces. The maximum connector horizontal force for each connector is identified to study the higher and lower force at which location of connector influences by the arrangement of HMFS system. The trend of horizontal connector force also studied in each arrangement maybe can be used in early approximation of horizontal connector force for expansion of the module after additional 4th module and higher at the top and bottom as symmetrical module is taken into account.

3.1. U-shaped configuration of HMFS arrangement

The maximum horizontal connector force of each connector for U-shaped configuration at various wave directions is shown in Fig. 4. At 0°, 30° and 45° of the wave directions, the higher horizontal connector force is at connector C3 and the lower at connector C1. The connector C2 has the higher horizontal connector force is at 60°, 85° and 90° of the wave directions. The connector C5 has the lowest horizontal connector force at 85° and 90° of wave directions. Overall value of horizontal connector force for U-shaped, the higher value is 5.23 MN on connecters C3 and C4 and the lower value is 0.32 MN at C1, meanwhile both value at 0° wave direction. Moreover, many connectors have a higher horizontal connector force value at the 0° wave direction, such as C1, C3, C4 and C6 and a lower horizontal connector force at the 90° wave directions on connectors C4, C5 and C6.

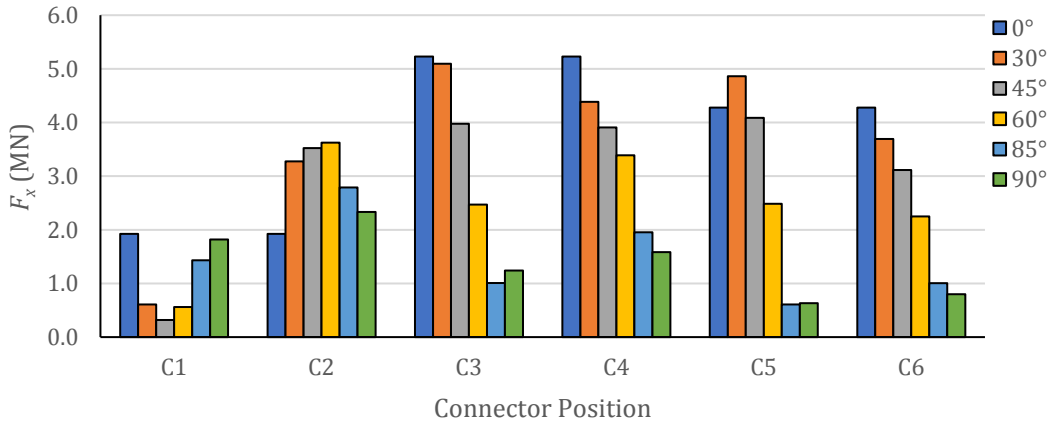

Fig. 4. Maximum horizontal connector force of each connector for U-shaped configuration at various wave directions.

There are two trend horizontal connector force for U-shaped configurations, firstly, at 0° wave direction, the horizontal connector force value at the top connector (C1, C3, C5) is similar to the bottom connector (C2, C4, C6). Initially, connectors C1, C3 and C5 at the top modules (M2, M4 and M6) is have similar value with connector C2, C4 and C6 at the bottom modules (M3, M5 and M7) at 0° wave direction, respectively. This is the connector at the top modules and bottom modules facing the wave direction 0°in same time as shown in Table 2 exhibit the similar value. The same applies by Li et al. (2023) that demonstrated the same horizontal connector load between two connectors facing the incident wave in the same time.

Table 2. Sequential orientation of the connector influenced by wave forces, highlighting the changing angle of the connector relative to the wave direction in in in 7U-shaped arrangement.

Wave direction	Sequential connector facing wave force	Angle connector facing wave force					
		C1 (DC\)	C2 (VC/)	C3 (P-)	C4 (P-)	C5 (P-)	C6 (P-)
0°	C5=C6, C3=C4, C1=C2	120°	60°	0°	0°	0°	0°
30°	C6, C4=C5, C2=C3, C1	90°	30°	-30°	-30°	-30°	-30°
45°	C6, C4, C5, C2, C3, C1	75°	15°	-45°	-45°	-45°	-45°
60°	C6, C4, C2, C5, C3=C1	60°	0°	-60°	-60°	-60°	-60°
85°	C6=C4, C2, C1, C3=C5	35°	-25°	-85°	-85°	-85°	-85°
90°	C6=C4, C2, C1, C3=C5	30°	-30°	-90°	-90°	-90°	-90°

Secondly trend, the if the top connector is higher value of horizontal connector force, the bottom will have a lower value, and vice versa for wave directions of 30°, 45°, 60°, 85° and 90°.The second trend is also given, in wave directions of 30° and 45°, the higher horizontal connector force at the top and the middle of the connector (C3) and followed by the first module facing wave (C5) while the lower of horizontal connector force is at the last module facing wave (C1). In addition, 60°, 85° and 90° of wave directions are opposite with 30° and 45°, the higher horizontal connector force at the bottom and the last module (C2) while follow by the middle module (C4). Other than that, the angle connector for C3, C4, C5 and C6 are the same angles due to the same connector orientation shown in Table 2, for example, wave direction of 30°, the parallel connector orientation of connector is C3, C4, C5 and C6 is -30°. However, the higher horizontal connector force is in connector C3, followed by connector C5, C4 and lastly C6. This finding is consistent with the findings of Liu et al. (2022), who demonstrate twelve square modules arranged in a linearly and side-by-side exhibit a higher horizontal connector load at inner modules compared to outer modules. They assert that this occurs due to the connector loads being influenced by load differences among adjacent modules, which caused by environmental conditions and other modules. Consequently, the connector loads can be effectively reduced by appropriately balancing the loads on adjacent modules.

3.2. VP-shaped configuration of HMFS arrangement

The maximum horizontal connector force of each connector for VP-shaped configuration at various wave directions is shown in Fig. 5. At 45°, 60°, 85° and 90° of the wave directions, the higher horizontal connector force is connector C5, while at 0° and 30°, the higher is at connector C3. The lower horizontal connector force on C4 at wave directions of 45° and 60° while on C3 at wave directions of 85° and 90°. Overall, the highest horizontal connector force is 4 MN on C3 and C4 at 0° of wave direction and the lowest is 0.35 MN at 30° of wave direction. Additionally, the higher horizontal connector force at 0° wave direction such as connectors of C2, C3, C4 and C6. The higher horizontal connector force of C1 is 30° wave directions at the center module while 60° of wave directions at connector C5. The lower of the connector is mostly at 30° of the wave directions on connectors C2, C4 and C6 at the bottom module (M3, M5, and M7).

There are three trends of higher horizontal connector force: Firstly, mostly higher horizontal connector force at the top connector arrangement module (C1, C3, C5) which has 0°, 30°, 45° and 60° of wave directions. The angles of connector facing the incident wave decreases on connectors C1, C3 and C5, which is below 30°, as indicated in Table 3. Besides, the findings of horizontal connector load indicates that for a linear arrangement, an increase in wave direction correspond to a decrease in horizontal connector loads. Thus, the top connectors of C1, C3 and C5 expressed lower connector angles facing wave force compared to connector C2, C4 and C6. It is similar to the findings of Song et al. (2023) and Wu et al. (2016) that the longitudinal load connecting two and three rectangular modules, respectively, experience an increase in wave direction given the decrease in longitudinal load.

Secondly, the 0° and 30° wave directions give a higher horizontal connector force on connector C3 which is the top middle module. However, in 45°, 60°, 85° and 90° the of wave direction on C5 at M6 are the outer module and end of top arrangement. Thirdly, in 85° and 90° wave direction the higher is C5 at the top module arrangement however the bottom connector (C2) is the second higher horizontal connector force. This is because the outer modules of the MFS, whether positioned at the front or rear, experience a higher horizontal connector load compared to the inner modules. The findings are similar to

Zhang et al. (2023) indicating that the connector in the middle module, assigned as connector C2 experiences lower loads compared to connectors C1 and C3, which are located in the outer modules linked three rectangular modules. Li et al. (2022) and Ren et al. (2021) also experienced the higher horizontal connection loads at the connector of outer modules, including initial modules and last modules, in comparison to middle modules for hexagonal and square for modular floating structures, respectively.

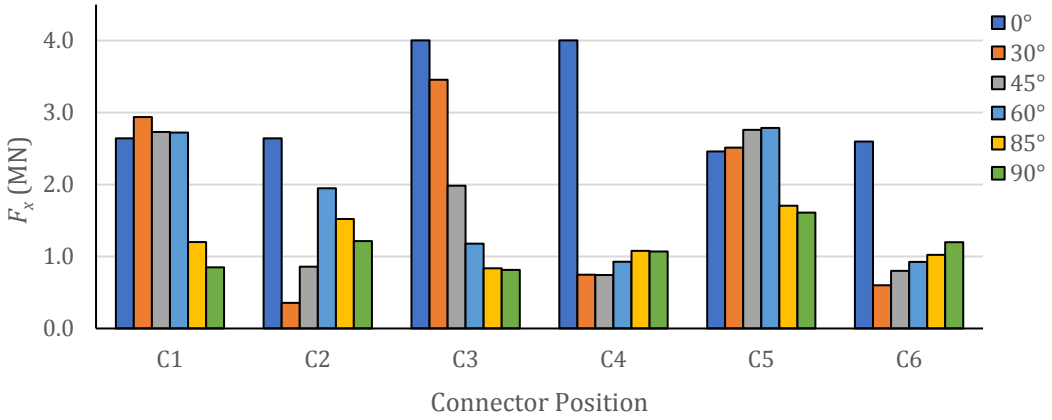

Fig. 5. Maximum horizontal connector force of each connector for VP-shaped configuration at various wave directions.

Table 3. Sequential orientation of the connector influenced by wave forces, highlighting the changing angle of the connector relative to the wave direction in 7VP-shaped arrangement.

Wave direction	Sequential connector facing wave force	Angle connector facing wave force					
		C1 (VC/)	C2 (DC\)	C3 (VC/)	C4 (DC\)	C5 (VC/)	C6 (DC\)
0°	C1=C2, C3=C4, C5=C6	60°	120°	60°	120°	60°	120°
30°	C2=C4=C6, C1, C3, C5	30°	90°	30°	90°	30°	90°
45°	C6, C4, C2, C1, C3, C5	15°	75°	15°	75°	15°	75°
60°	C6, C4, C2, C1, C3, C5	0°	60°	0°	60°	0°	60°
85°	C6, C4, C2, C1, C3, C5	-25°	35°	-25°	35°	-25°	35°
90°	C6, C4, C2, C1, C3, C5	-30°	30°	-30°	30°	-30°	30°

3.3. VV-shaped configuration of HMFS arrangement

Fig. 6 shows the maximum horizontal force of each connector for a VV-shaped configuration at various wave directions. At 0°, 85° and 90° of the wave directions, the higher horizontal connector force is at connector C3 while at 30°, 45° and 60° of the wave directions, the higher horizontal connector force is at connector C5. Connector C4 receives the majority of the lower horizontal connector force value. Overall value of horizontal connector force for VV-shaped, the higher value is 4.77 MN on connecter C3 at 0° wave direction and the lower value is 0.14 MN at C6 at 90° wave direction. In addition, many connectors have a higher F_x value at the 30° wave direction, such as C1, C2, C5 and C6 as the connectors attached at the center module (M1) and outer module facing the wave (M6, M7). The lower F_x force at the 90° wave directions on connectors C4, C5 and C6 because HMFS linked M1, M3, M5 and M7 illustrates as linear arrangement. The lower connector F_x forces at C1, C3 and C5 are 30°, 60°, and 90°. Due to linear arrangement at the bottom (M3, M5 and M7), the connector F_x force at C2, C4 and C6 is lower and higher horizontal connector force at C1, C3 and C5 for the top symmetrical loop arrangement module (M2, M4 and M6).

The higher horizontal connector force at the top arrangement has two trends: at the outer module (C5) for wave directions of 30°,45° and 60°, while 0°, 85° and 90° of wave directions at the connector on the middle module (C3). The lower horizontal connector force at the bottom arrangement also has two trends: at outer module (C6) for wave directions 45°, 60°, 85°, and 90° while 0° and 30° of wave directions are at the middle module (C4). The connector of C1, C3 and C5 shown the angle connector facing wave force shifting to below 30° incident waves for wave direction 0°, 30°, and 45° shown in Table 4. In contrast, the connector of C2, C4 and C6 is facing wave directions 0°, 30°, and 45° shifting to above 30° incident waves, as indicated in Table 4. This finding confirmed by Otto et al. (2019), indicating the hexagonal modular floating structures should avoid the environmental condition below 30° as given the higher connector loads and also compared with the square modular floating structures.

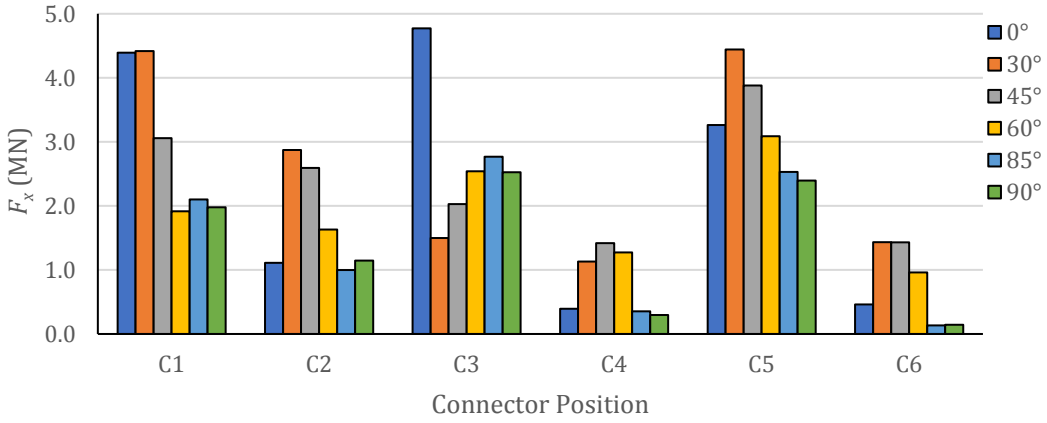

Fig. 6. Maximum horizontal connector force of each connector for VV-shaped configuration at various wave directions.

Table 4. Sequential orientation of the connector influenced by wave forces, highlighting the changing angle of the connector relative to the wave direction in in 7VV-shaped arrangement.

Wave direction	Sequential connector facing wave force	Angle connector facing wave force					
		C1 (VC/)	C2 (P|)	C3 (VC/)	C4 (P|)	C5 (VC/)	C6 (P|)
0°	C2=C4=C6, C1, C3, C5	30°	90°	30°	90°	30°	90°
30°	C6, C4, C2, C1, C3, C5	0°	60°	0°	60°	0°	60°
45°	C6, C4, C2, C1, C3, C5	-15°	45°	-15°	45°	-15°	45°
60°	C6, C4, C2, C1, C3, C5	-30°	30°	-30°	30°	-300	30°
85°	C6, C4, C2, C1, C3, C5	-55°	5°	-55°	5°	-55°	5°
90°	C6, C4, C2, C1, C3, C5	-60°	0°	-60°	0°	-60°	0°

However, in wave direction of 85° and 90°, the angle connectors facing the wave force 0˚ and close to 60˚ encounter the higher horizontal connector load. The findings of Li et al. (2022) different from these research findings as the higher horizontal connector loads in linear arrangements is 60°, followed by 0° and 30° linked five hexagonal modular floating structures. They stated that an incidence wave direction of 60^0 results in higher connector load due to a less significant shielding effect among modules. Additionally, Li et al. (2023) studied four hexagonal modular floating structures linked in L-shaped oblique arranged in one central module, mention that the yaw, sway and heave all tends to be higher with the incident wave direction of 0° or 60°. In their findings, they also indicate the higher horizontal connector load towards 0° and 60° compared to 30° and 90°. Thus, hexagonal shape should consider that the wave direction of 0° and 60° will be experience the higher horizontal connector loads.

3.4. Design recommendations for real-world implementations

In the real world, a hexagonal module positioned with its vertex side facing the incident wave was installed at Hakata Bay, Japan, in 2011 to evaluate its performance as floating offshore wind turbine (Watanabe et al. 2017). The hexagonal modular floating structure also has been installed in Punggol Eco Town in Singapore, serving as a sustainable waterfront community for tropical regions (Wong et al. 2013). In addition, Paul Ridden (2018) reported that twenty-eight hexagonal module floating structures made by recycled plastic was assembled at Rotterdam harbor, Netherlands, with the vertex side oriented towards incident wave on July 2018. The hexagonal modules served as the floating park that the hexagonal module being planted with greenery, benches for visitors and habitat for micro and macro fauna, such as snail, beetles, fish and birds. Furthermore, the small hexagonal modular floating structure has also functioned as a floating dock. The HMFS has also been installed in the Republic of Djibouti, Africa, operating as a fish farm (Piccolotti and Lovatelli 2013). Currently, China has installed a huge hexagonal module with 434 photovoltaic panels (CGTN 2024), functioning as wave-resistant floating photovoltaic platform located in waters near the southern part of Shandong, China. They indicated that a module has been installed to the testing process, with additional modules to be added later, resembling a giant honeycomb to provide optimal stability. Meanwhile, the HMFS function as floating cities is still in conceptual designs. The conceptual design of floating cities is presented by Lister and Muk-Pavic (2015), Stanković et al. (2021), and Shihy (2024).

This research studied two types of HMFS arrangement: linear arrangement and staggered arrangement. In the context of linear arrangements, the parallel sides of hexagon can be aligned in a straight line, as illustrated

in linear arrangement; however, the vertex sides cannot arrange in a straight line. Furthermore, the linear arrangement can create two arrangements: firstly, the parallel side of hexagon facing the incident wave, as illustrated in linear arrangement and second, the vertex side facing the incident wave, represented as one apart in VV-shaped arrangements. This research identifies the connector that aligns with the incident wave as a parallel connector in horizontal direction (P-) exhibiting the highest horizontal connector loads in linear arrangements, especially in 0° wave direction. In contrast to the parallel connector in the vertical direction (P|), the lowest horizontal connector loads are indicated in the findings of VV-shaped arrangement. Besides, the shifting of the angles connector facing the incident wave in the parallel connector in vertical direction (P|) has 0° wave direction did not demonstrate a higher horizontal connector load in certain arrangements. Therefore, the vertex side facing incident wave applied the parallel connector in vertical direction is a good selection for linear arrangements. The linear arrangement is commonly used in breakwater, floating dock and renewable floating system, such as solar panels and wind turbines.

The vertex side facing the incident wave has also been recommended in designing the HMFS arrangements, which adopted the arrangement of side-by-side and circular configuration. The hexagonal side facing the incident wave influenced the number and layout of HMFS arrangements. As the finding discovers that two connectors, such as horizontal direction (P-) and vertical angles exhibit the higher horizontal connector loads. Likewise, the symmetrical conceptual design of MFS, creates the parallel side facing incident waves only can be arranged in seven modules: one in the central, three modules acting as arm, that three modules positioned top and two module bottoms, as illustrated in U-shaped (7U) utilized three directions of connector: horizontal connectors in horizontal direction (P-), vertical angles and diagonal angles. The VP-shaped arrangement connecting all seven modules utilizes two directions of connector: vertical angles and diagonal angles. Meanwhile, the VV-shaped utilized two directions of connector: vertical connectors in horizontal direction (P|), and vertical angles. However, only the vertical angles indicate the higher horizontal connector loads.

4. Conclusions

The present work proposes a HMFS connected to seven modules with a ball connector. The multi-floating structure hydrodynamics interaction effect and connector coupling effect were considered. The effect of wave direction and location of connector on the different arrangements of HMFS was investigated. The conclusion has been summarised as follows:

- The 0° wave direction gives a higher horizontal connector force for the HMFS system in all arrangements, for instance, U-shaped, VP-shaped and VV-shaped arrangement of HMFS.
- The U-shaped arrangement has the higher horizontal force of connector among three arrangements. U-shaped arrangement also has symmetrical F_x force value, the top connector and the bottom connector have the same connector force within the same location connector symmetrically.
- The parallel side hexagonal facing wave continues or changing the other sides will still get the VP-shaped layout however, in the VV-shaped arrangement the vertices facing wave given more to the L-shaped layout.
- The horizontal force at VV-shaped is higher horizontal force compared to VP-shaped as the difference between the vertices and sides facing wave direction 0°.
- The designer should choose the best arrangement for the hexagonal shape of the modular floating structure because each arrangement has its own suitable function. Then, next decision knowing the maximum horizontal connector force pattern in chosen the best arrangement due connector is also crucial for safety and stability for modular floating structure.

The determination of horizontal load in various HMFS arrangements allows early estimation of the connector load according to its HMFS functionality and HMFS layout. The identification of the higher horizontal connector load in various wave directions enables the connector and VLFS designer to focus to the 0° and 60° of wave directions when pursuing the conceptual design of the VLFS in hexagonal shape. As Otto et al. (2019) mention that designer should avoid the conceptual design of HMFS arrangement in wave direction below 30° as generated the higher horizontal connector load. Other that than, the comparison of horizontal connector load in various wave directions allowing identifying the impact of the changing angle of the connector relative to the wave direction in in HMFS arrangement.

For future recommendation, the simulation performed in this research is a limited selected case on 8s at a short-wave period at all seven arrangements. Thus, the simulation work should be extended for more wave period including short wave periods of 4s-8s and longer wave periods of 10s to 20s to enhance the safety connector and take into account that it effected the stability of HMFS. Other than that, the simulation performed in this research is limited to the determination of horizontal connector load increasing in seven numbers of modules, as the MFS has a higher number of modules, especially in the conceptual design of the floating city. Thus, the horizontal connector load should be extended further up to 20 modules as the limitation number of modules created in ANSYS software, then will confident in the early approximation of horizontal connector load.

References

ANSYS (2013). Aqwa Theory Manual, Release 15.0. ANSYS Inc., Canonsburg, PA.

Azlan NHA, Shaharuddin NMR, Ali A (2024). Influence of connector forces on the expansion configuration of a hexagonal modular floating structure. *5th International Conference on Advanced Engineering Technologies,* Bayburt, Türkiye, 1211–1217.

CGTN (2024). China's Wave-Resistant Floating Photovoltaic Platform to Enter Experimental Phase [Broadcast]. https://english.www.gov.cn/english.www.gov.cn/news/202410/03/content_WS66fe35cec6d0868f4e8eb7ff.html [accessed 05-12-2024].

Acknowledgements

This research has previously been presented at the 5th International Conference on Advanced Engineering Technologies (ICADET'24) held in Bayburt, Türkiye, on September 25-27, 2024. Extended version of the research has been submitted to Challenge Journal of Structural Mechanics and has been peer-reviewed prior to the publication.

Funding

The authors received no financial support for the research, authorship, and/or publication of this manuscript.

Conflict of Interest

The authors declared no potential conflicts of interest with respect to the research, authorship, and/or publication of this manuscript.

Author Contributions

All of the authors made substantial contributions to conception and design, or acquisition of data, or analysis and interpretation of data; were involved in drafting the manuscript or revising it critically for important intellectual content; and gave final approval of the version to be published.

Data Availability

The datasets created and/or analyzed during the current study are not publicly available, but are available from the corresponding author upon reasonable request.

Dai J, Hellan Ø, Want A, Ang KK (2021). Modular multi-purpose floating structures for space creation. *Lecture Notes in Civil Engineering*, 158, 257–271.

Ding J, Wu YS, Zhou Y, Ma XZ, Ling HJ, Xie Z (2020). Investigation of connector loads of a 3-Module VLFS using experimental and numerical methods. *Ocean Engineering*, 195(10), 106684.

Hamamoto T, Fujita, KI (2016). Water tank experiment of shape-variable floating structures. *Journal of Structural and Construction Engineering*, 81(724), 1039–1049.

Hongtao Y, Gang C, Wei Z, Yan Y, Yuhan W, Chao W (2020). Design for flexible connector of multi-floating structure. *Proceedings of the ASME 2020 39th International Conference on Ocean, Offshore and Arctic Engineering.*

Ikegami K, Matsuura M, Wada Y, Zhang G (2007). Response characteristics of a multi-connected floating body system in waves. *Proceedings of the 26th International Conference on Offshore Mechanics and Arctic Engineering,* 1–10.

Jiang D, Tan KH, Dai J, Ang KK, Nguyen HP (2021a). Behavior of concrete modular multi-purpose floating structures, *Ocean Engineering*, 229, 108971.

Jiang D, Tan KH, Dai J, Ang KK, Nguyen HP (2021b). Research and development in connector systems for very large floating structures. *Ocean Engineering,* 229, 108971.

Lan Y, Run PL, Zhi S (2004). A numerical and experimental study on dynamic responses of MOB connectors. *Proceedings of the 14th International Offshore and Polar Engineering Conference*, 636–643.

Li Y, Ren N, Li X, Ou J (2022). Hydrodynamic Analysis of a Novel Modular Floating Structure System Integrated with Floating Artificial Reefs and Wave Energy Converters. *Journal of Marine Science and Engineering*, 10(8), 1091.

Li Y, Li X, Ren N, Ou J (2023). Hydrodynamic responses of a novel modular floating structure system with multi-direction expansion. *Journal of Offshore Mechanics and Arctic Engineering*, 145(3), 1-25.

Li Y, Ren N, Cai W, Liu Y, Ou J (2024). Experimental and numerical study on dynamic responses of a TLP-Type 2 modular floating structure system. *Ocean Engineering*, 313(3), 119427.

Lister N, Muk-Pavic E (2015). Sustainable artificial island concept for the Republic of Kiribati. *Ocean Engineering*, 98, 78–87.

Liu YQ, Ren N, Ou, J (2022). Investigation on Effects of mooring line fractures and connector failures for a hybrid modular floating structure system. *China Ocean Engineering*, 36(6), 880–893.

Otto W J, Waals O J, Bunnik THJ, Cresp J (2019). Optimization of wave induced motions and forces on a floating island. *Proceedings of the 29th International Ocean and Polar Engineering Conference*.

Park HJ, Kim JS, Nam BW (2023). Numerical analysis for motion response of modular floating island in waves. *Journal of Ocean Engineering and Technology*, 37(1), 8-19.

Paul R (2018). Floating park built using recycled waste plastic opens in Rotterdam. *New Atlas.* https://newatlas.com/recycled-park-rotterdam/55441 [accessed 05-12-2024].

Piccolotti F, Lovatelli A (2013). Construction and installation of hexagonal wooden cages for fish farming: A technical manual. In *FAO Fisheries and Aquaculture Technical Paper*, No. 576, Rome, Italy.

Ren N, Wu H, Liu K, Zhou D, Ou J (2021). Hydrodynamic analysis of a modular floating structure with tension-leg platforms and wave energy converters. *Journal of Marine Science and Engineering*, 9(4), 424.

Riggs HR, Ertekin RC, Mills TRJ (1998). Wave-induced response of a 5-module mobile offshore base. *Ocean Space Utilization Symposium,* Lisbon, Portugal.

Shihy AA (2024). A new approach for configuring modular floating cities: Assessing modular floating platforms by means of analytic hierarchy process. *City, Territory and Architecture*, 11, 8.

Song X, Liu W, Wu H (2023). Investigation on load characteristics of hinged connector for a large floating structure model under wave actions. *Journal of Marine Science and Engineering*, 11(4), 786.

Stanković J, Krasić S, Mitković P, Nikolić M, Kocić N, Mitković M (2021). Floating modular houses as solution for rising sea levels – A case study in Kiribati island. *Proceedings of the 39th International Conference on Education and Research in Computer Aided Architectural Design in Europe (ECAADe*), Novi Sad, Serbia, 1, 161–170.

Vincenzo B (2023). Modelling and design of a flexible connector for modular floating platforms. *Diploma thesis*, Politecnico Di Torino, Corso Di Laurea Magistrale in Ingegneria Meccanica, Torino, Italy.

Watanabe E, Utsunomiya T, Wang CM (2004). Hydroelastic analysis of pontoon-type VLFS: A literature survey. *Engineering Structures*, 26(2), 245–256.

Watanabe K, Ohya Y, Uchida T, Nagai T (2017). Numerical prediction and field verification test of wind-power generation potential in nearshore area using a moored floating platform. *Journal of Flow Control, Measurement & Visualization*, 5(2), 21–35.

Wong LH, Tan HS, Wang CL, Lim H, Ho HC, Wang CM, Tay ZY, Gao RP (2013). Floating wetlands at Punggol. *IES Journal Part A: Civil and Structural Engineering*, 6(4), 249–257.

Wu L, Wang Y, Xiao Z, Li Y (2016). Hydrodynamic Response for flexible connectors of mobile offshore base at rough sea states. *Petroleum Exploration and Development*, 43(6), 1089–1096.

Xiaozhou M, Guohai D, Yanjun M, Yufei W, Fang Y, Xiong L, Luyao Z (2024). Experimental study on the hydrodynamic performance of a flexible connected double-module floating structure. *Journal of Offshore Mechanics and Arctic Engineering*, 146(5), 051703.

Zhang X, Wang J, Li L, Sun S, Wang Z (2023). Load analysis of connectors for floating structures at sea. *Frontiers in Computing and Intelligent Systems*, 5(1), 95-99.

Challenge Journal of Structural Mechanics

Research Article

Improving bond performance of 3D-printable earth-based mortar reinforced with jute fibers

Yeşim Tarhan [a,*], İsmail Hakkı Tarhan [b], Arnaud Perrot [c]

[a] *Technical Sciences Vocational School, Ardahan University, 75000 Ardahan, Türkiye*
[b] *Department of Civil Engineering, Tokat Gaziosmanpaşa University, 60000 Tokat, Türkiye*
[c] *Research Institute Dupuy De Lôme, University of Southern Brittany, F-56100 Lorient, France*

ABSTRACT

3D printing technology has transformed the construction industry by enabling rapid and cost-effective production of complex geometries. However, it faces significant challenges, including sustainability concerns due to cement's environmental impact and reinforcement issues arising from the incompatibility of traditional steel. These challenges necessitate the development of innovative material solutions. This study aims to enhance the bond strength between sustainable earth-based mortar and jute fibers used as reinforcement in 3D printed structures by exploring the effects of different treatments and compositions. Bond strength was evaluated by considering the effect of different treatments on the resistance of the fiber to being pulled out of the mortar. Pull-out tests were conducted on specimens with varying compositions and treatments. Results demonstrated substantial improvement in bond performance; specifically, the reference sand-free earth-clay mortar exhibited the lowest interfacial shear strength of 0.30 MPa. The most remarkable enhancement was observed in specimen which jute fibers pre-treated by immersion in mud slurry, which showed a 147% increase, reaching an interfacial shear strength of 0.74 MPa. Combining sand addition and fiber pre-treatment, however, did not yield additional benefits. These results indicate that simple, cost-effective local treatments can notably enhance fiber-matrix bond strength in 3D-printed earth-based structures without necessitating additional equipment or significant expense.

ARTICLE INFO

Article history:
Received – October 31, 2024
Revision requested – January 17, 2025
Revision received – April 13, 2025
Accepted – April 28, 2025

Keywords:
3D printing construction
Earth-based mortar
Jute fiber
Pull-out test
Bond strength

Citation: Tarhan Y, Tarhan İH, Perrot A (2025). Improving bond performance of 3D-printable earth-based mortar reinforced with jute fibers. *Challenge Journal of Structural Mechanics*, 11(2), 99–105.

1. Introduction

The construction industry contributes significantly to environmental problems such as high CO_2 emissions, depletion of natural resources, and intensive energy consumption, especially due to the calcination process of cement production (Mahmud et al. 2025; Mohamad et al. 2025; Bulut 2024; Güney and Yıldızel 2024; Macherla 2023; Melià et al. 2014). In response, earth-based materials are increasingly being considered due to their environmental friendliness and lower energy requirements for production. Recent studies have focused on improving the engineering properties and durability of these natural materials (Nagaraj and Muguda 2020). This renewed interest is in line with broader trends towards sustainable construction practices, as evidenced by the growing popularity of materials such as rammed earth (Sposito and Scalisi 2017).

3D printing technology has emerged as a promising method in the construction industry, allowing for rapid production, cost savings, and intricate architectural designs. Its integration with earth-based materials has attracted considerable attention due to their sustainability and accessibility (Shahrubudin et al. 2019; Ferretti et al.

* *Corresponding author*. Tel.: +90-478-211-7575 ; E-mail address: yesimtarhan@ardahan.edu.tr (Y. Tarhan)
ISSN: 2149-8024 / DOI: https://doi.org/10.20528/cjsmec.2025.02.004

2022; Gomaa et al. 2021; Perrot et al. 2016; Tarhan and Perrot 2023; Tarhan et al. 2024). Perrot et al. (2016) pioneered the field of 3D-printable earth-based materials, successfully demonstrating the 3D printability of earth-based mixtures for the first time. Gomaa et al. (2021) developed a novel dual-ram extruder system for 3D printing cob, improving extrusion rate, continuity, consistency, and mobility while also optimizing the cob mixture for 3D printing by adjusting water content. Ferretti et al. (2022) investigated the long-term mechanical properties of earthen mixtures for 3D printing, examining the effects of rice husk shredding on compressive strength and stiffness.

However, reinforcement is a significant challenge that needs to be addressed but is mainly ignored in 3D-printable earth-based materials. Natural fibers such as jute (Loccarini 2017; Sen and Saha 2024; Tarhan and Perrot 2023; Tarhan et al. 2024), sisal (Alves Fidelis et al. 2013; Yadav et al. 2019; Zavaleta et al. 2024), date palm (Abdeldjebar et al. 2018; Benzerara et al. 2021; Dawood and Alqaissi 2024; Taallah and Guettala 2016), and bamboo (Sen and Saha 2024) are utilized to enhance the mechanical properties of earth-based construction materials. Nevertheless, the bond between such fibers and clay-rich printable mortars remains a key limitation, often leading to inadequate stress transfer and reduced structural efficiency.

Taallah and Guettala (2016) examined untreated and alkali-treated date palm fibers in compressed earth blocks. Alkali treatment slightly improved fiber performance but decreased overall block strength and thermal insulation compared to non-fiber blocks. The study highlights the complex effects of fiber treatments on earth-based materials. Ramesh et al. (2017) also examine the use of plant fibers in construction, noting their potential in composites for sustainable development and the improved mechanical properties they can provide. Loccarini et al. (2017) investigated using jute fabric as a natural reinforcement for rammed earth structures. The study examined the adhesion capacity of jute fabric with an earth-gypsum matrix through peeling tests and single lap joint tests. Results showed that jute fabric reinforcement significantly increased the bearing capacity and kinematical ductility of rammed earth arches. Tarhan and Perrot (2023) proposed a novel technique using untreated jute fabric to reinforce 3D-printed earth-based composites. They found that jute fabric reinforcement significantly improved the ductility and compressive strength of 3D-printed earth-based samples. In a follow-up study, Tarhan et al. (2024) investigated the effects of earth slurry-treated jute fibers on the flexural, compressive, and interlayer strength of 3D-printed earth-based beam samples. This treatment resulted in notable improvements in mechanical properties, highlighting the significant impact of fiber treatment on the performance of reinforced 3D-printed earth-based materials. The study also emphasized that further measures should be investigated to increase the bond strength of jute fabric and earth-based mortar. Sen and Saha (2024) evaluated bitumen-treated jute and bamboo fibers for retrofitting rammed earthen houses against seismic loads. Their novel approach using bitumen-treated bamboo strips as external reinforcement and L-shaped corner reinforcements significantly enhanced structural strength and ductility, with seismic resistance improving up to 6.81 times compared to unreinforced structures. However, Archila et al. (2018) noted that while plant fibers can improve certain material properties, they may also introduce new complexities that necessitate further research and innovation.

Although previous studies have investigated the use of natural fibers in earth-based construction materials, there is still a limited understanding of how these fibers interact with earth-based mortar specifically in the context of 3D-printed structures. In particular, the mechanisms governing fiber-matrix bonding and the influence of fiber treatments in 3D printing remain largely unexplored. Addressing this gap, the present study aims to examine the key factors that influence the bond strength between jute fibers and 3D-printable earth-based mortars. To achieve this, jute fibers were pre-treated by immersion in clay (mud) slurry - the binder component of the mortar - before being placed between printed layers. Pull-out tests were then conducted to assess the bond strength of both untreated and slurry-treated fibers in two different mortar compositions. By doing so, this research contributes new quantitative insights into how sand addition and fiber pre-treatment affect interfacial bonding, thereby advancing the material design of sustainable, fiber-reinforced 3D-printed structures.

2. Materials and Method

This section details the materials used in the study, the preparation of specimens, and the methods employed for testing bond strength between jute fibers and earth-based mortars. The focus is on two main variables: the composition of the earth-based mixture and the pre-treatment of jute fibers.

2.1. Materials

In the current study, the same natural materials used in previous studies (Tarhan and Perrot 2023; Tarhan et al. 2024) were adopted to prepare the earth-based mortar mixtures. These include silt-containing raw earth, clay-rich quarry wash mud, and fine silica sand with a maximum particle diameter of 1 mm and a bulk density of 2.26 g/cm^3. The quarry wash mud, acting as the main binder, had a specific surface area of 10 m^2/g, a density of 2.65 g/cm^3, a plasticity index of 29, a liquid limit of 62.8%, and a plastic limit of 34.1%. To evaluate the influence of sand, a second sand-free mixture was also prepared, replicating the formulation reported by Tarhan et al. (2024) but omitting silica sand. Since sand represents the largest particle size fraction in the mixture, its inclusion was expected to prominently affect fiber-mortar interaction, especially considering the small dimensions of the pull-out test specimens. Compositions for both mixtures are listed in Table 1.

The jute fibers used were natural, untreated, and sourced commercially. For the treatment group, fibers were immersed in a clay (mud) slurry for 15 minutes, then gently wiped to remove excess slurry and dried at ambient conditions (20 °C, ~50% RH) for 24 hours. Specimens were classified into four groups as shown in Table 2.

Table 1. Proportions of the mixtures.

3D printable mixes	Components (%)			
	Raw earth	Quarry wash	Sand	Water
1. Mixture (with sand)	44	16	40	21
2. Mixture (sand-free)	64	36	-	28

Table 2. Description of the specimen groups based on mixture composition and fiber treatment.

Group	Mixture composition	Fiber treatment
EC-F	Earth + Clay (No Sand)	Untreated
EC-MF	Earth + Clay (No Sand)	Mud slurry–treated
ECS-F	Earth + Clay + Sand	Untreated
ECS-MF	Earth + Clay + Sand	Mud slurry–treated

To assess the printability of both mixtures, fall cone tests were conducted in accordance with EN ISO 17892-6 (2017). This was achieved by measuring the penetration depth of a cone under an applied load. The cone tip was placed on the surface of the mixture and released for approximately five seconds, allowing sufficient time for penetration to occur. The resulting data demonstrated penetration depths of 19.8 mm for the sand-blended mix and 16.5 mm for the sand-free mix. Both of these mixtures exhibited excellent printability characteristics for use in 3D printing. Fig. 1 shows one of the 3D-printed beam-shaped samples reinforced with jute textiles.

Fig. 1. Earth-based specimens equipped with 3D-printed jute fabric (Tarhan and Perrot 2023).

Fiber diameters –both untreated and slurry-coated– were measured using an optical microscope (Leica DM750), and representative images are provided in Fig. 2. Eight jute fiber samples were utilized in sand-blended and sand-free mixes, untreated, and immersed in mud slurry for the pull-out test. Some of the fiber diameters measured by optical microscopy are shown in Fig. 2.

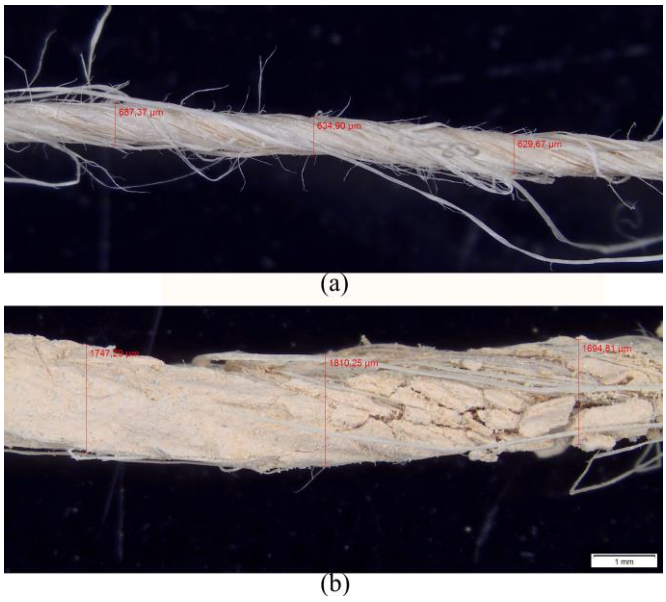

Fig. 2. Optical microscope measurements:
(a) Diameter of the untreated jute fiber;
(b) Jute fiber immersed in mud slurry.

2.2. Sample preparation and pull-out test

Pull-out test specimens were prepared using a custom designed PVC mould as shown in Fig. 3. The mould consists of two laser-cut PVC plates: the lower plate contains a 1 mm diameter hole to center the fiber, the upper plate forms a 5 mm diameter cylindrical cell for the earth mixture. Prior to casting, the upper mold surfaces were lubricated with a thin layer of Vaseline to facilitate demolding. The jute fiber was threaded through the mold hole and centered so that approximately 15 mm of its length was embedded. The earth-based mixture was then poured into the mold and gently compacted by

hand. After casting, the specimens were left in the mold for 24 hours under laboratory conditions (20 °C and 50% relative humidity). They were then demolded and further oven dried at 60 °C for 15 days to ensure complete moisture removal and strength gain, following the methodology of Tarhan and Perrot (2023).

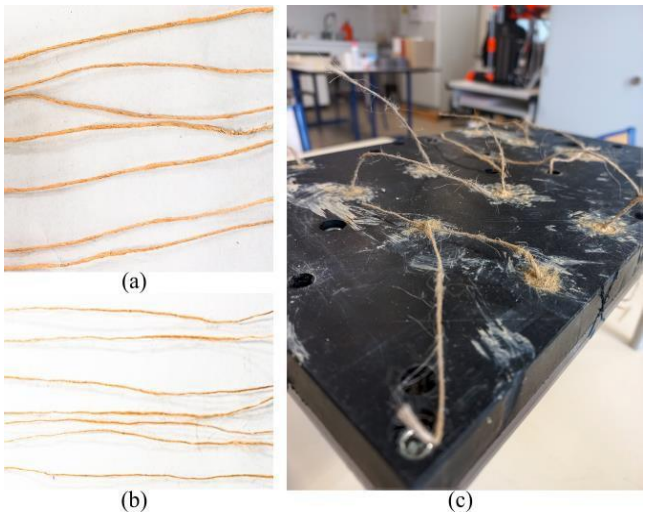

Fig. 3. (a) Muddy jute fibers; (b) Untreated jute fibers; (c) The tool used to create specimens, and placing jute fiber and earth-based mortars.

For mechanical testing, tensile tests were performed using a universal testing machine (MTS Insight Series) equipped with a 50 N load-cell. Each jute fiber was clamped in pneumatic grips to prevent slippage and pulled at a constant displacement rate of 1 mm/min until complete debonding occurred. Testing was carried out under controlled laboratory conditions (~20 °C, 50% RH). The average interfacial bond strength was considered as the apparent interfacial shear strength (*IFSS*), assuming a uniform interfacial stress distribution at the fiber/earth interface. It was calculated according to Lecompte et al. (2015) using the Eq. (1):

$$IFSS = \frac{F_{bond}}{\pi.t.D_f} \quad (1)$$

where F_{bond} is the maximum pull-out force (N), t is the matrix height (mm), and D_f is the average fiber diameter (mm) placed in the earth-based mixture (Fig. 4). This calculation provides a standardised measure of interfacial bonding performance, allowing comparison between different mixture compositions and fiber treatments, and is critical for understanding the efficiency of load transfer between the fiber and the surrounding matrix.

Fig. 4. Pull-out test device and crack development in the sample.

3. Results and Discussion

Table 3 and Fig. 5 present the results from the pull-out test, including maximum force, maximum elongation, *IFSS*, and the percentage increase in bond strength compared to the reference EC-F specimens.

Table 3. Results of the pull-out test.

Group	Sample name	Force (N)	Extension (mm)	*IFSS* (MPa)	Average *IFSS* (MPa)	Increase (%)
1	EC-F (1)	5.42	1.58	0.33	0.30	-
	EC-F (2)	4.29	1.43	0.26		
2	ECS-F (1)	8.54	1.38	0.52	0.57	90
	ECS-F (2)	9.96	1.45	0.61		
3	EC-MF (1)	13.64	2.17	0.84	0.74	147
	EC-MF (2)	10.50	1.57	0.64		
4	ECS-MF (1)	9.56	2.55	0.59	0.56	87
	ECS-MF (2)	8.47	1.03	0.52		

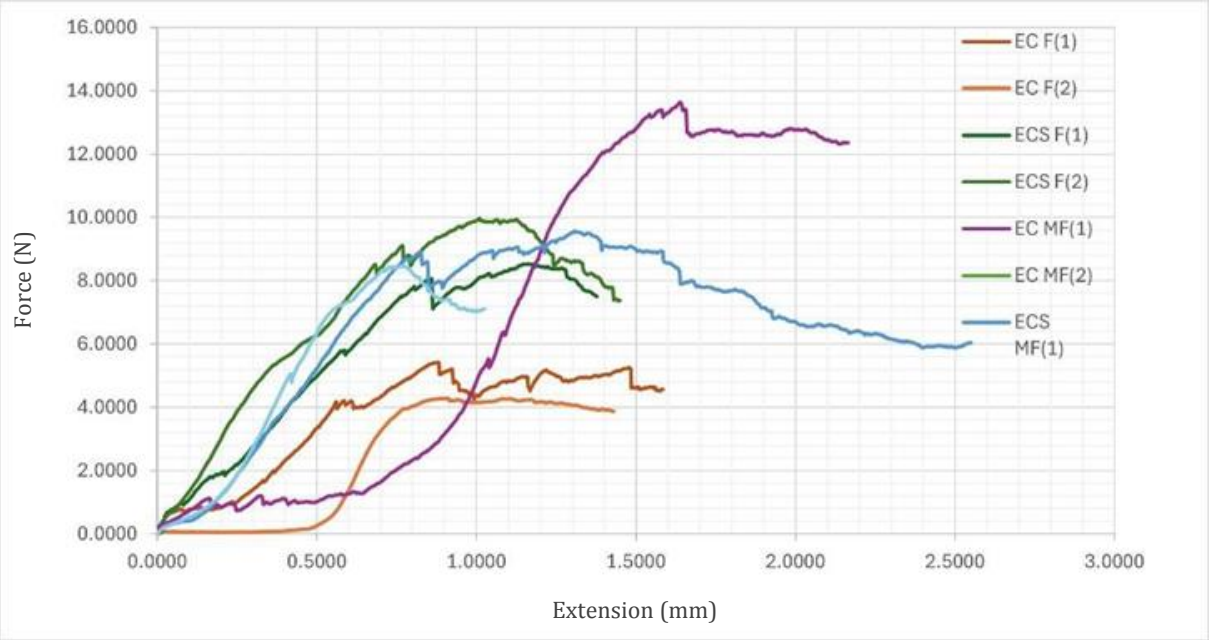

Fig. 5. Pull-out test results.

The reference group (EC-F), consisting of earth and clay without sand and using untreated jute fiber, showed the lowest average *IFSS* at 0.30 MPa. The addition of sand to the mix (ECS-F) resulted in a significant 90% increase to 0.57 MPa. This improvement is probably due to the increased frictional resistance provided by the sand particles at the fiber-matrix interface. The presence of sand can create a more tortuous path during fiber extraction, increasing the mechanical interlock and the energy required for debonding – defined here as the resistance of the fiber to being pull-out of the mortar. These findings are consistent with the findings of Tang et al. (2010), who demonstrated that increasing sand content in soil composites improved sliding resistance of fibers due to higher superficial roughness. Similarly, Abdi et al. (2011) showed that encapsulating reinforcement in sand layers within clay matrices significantly increased pull-out resistance.

The most significant improvement was observed in the EC-MF group where the jute fibers were pre-treated by immersion in clay slurry. This group achieved an average *IFSS* of 0.74 MPa, an increase of 147% over the reference. Two main mechanisms may explain this improvement: (i) the clay slurry may fill micro voids on the fiber surface, increasing the effective contact area; and (ii) the pre-treatment may improve the physico-chemical compatibility between the fiber and the clay-based matrix, resulting in a stronger bond. Similar positive effects of slurry treatments were reported by Tarhan et al. (2024), who found that jute fibers treated with earth slurry improved both flexural and compressive strength in 3D printed earth-based elements. Fagone et al. (2019) showed that jute fabric reinforcement improved adhesion and ductility in rammed-earth arches, although bond strength was not quantified in this study. Fode et al. (2025) revealed that bentonite slurry-treated sisal fibers embedded in cementitious matrices exhibited improved interfacial bonding and mechanical strength.

Interestingly, the combination of sand addition and fiber pre-treatment (ECS-MF) resulted in an average *IFSS* of 0.56 MPa, an increase of 87% over the reference. However, this was slightly less than the improvement achieved by pre-treatment alone (EC-MF), suggesting that the effects of the two methods may not be additive. A possible explanation is that there may be opposing mechanisms at work. While sand increases friction and surface roughness at the interface, the slurry coating may smooth or modify the fiber surface, thereby reducing the ability of the matrix to compact tightly around the treated fibers. In addition, material-specific limitations –such as the binding capacity of the clay matrix or the tensile strength of the jute fiber– may impose a ceiling beyond which further improvements are not possible, even with multiple interventions. This interpretation is consistent with Archila et al. (2018), who noted that combining reinforcement strategies in earthen materials can lead to complex interactions that do not necessarily yield cumulative benefits.

These results demonstrate that both sand addition and fiber surface treatment can significantly improve fiber-matrix bonding, but clay slurry treatment emerges as a more effective strategy, particularly for small-scale 3D printing applications. Importantly, the performance of the sand-free, fiber-treated group (EC-MF) highlights a simple and innovative approach that relies solely on readily available, low-cost materials without the need for sand or advanced processing. This makes the method highly relevant for sustainable construction, particularly in regions where sand is scarce or expensive.

4. Conclusions

This study investigates the bonding between jute fiber and earth-based 3D printable mortar via pull-out tests on different fiber conditions (untreated and mud slurry-treated) and mixture compositions.

The results indicate that interfacial shear strength can be substantially improved -from 0.30 MPa to 0.74 MPa (a 147% increase) - through clay slurry treatment of jute fibers, offering an accessible and cost-effective reinforcement method. Although sand addition alone led to a 90% increase, combining both strategies yielded no further improvement, suggesting a performance ceiling likely governed by material limits. These findings highlight the effectiveness of targeted, single interventions in enhancing fiber–matrix interaction and offer practical guidance for optimizing the mechanical performance of sustainable, 3D-printed earthen structures.

However, it was found that when the fibers were pretreated, the presence of sand may inhibit further bond development - possibly due to reduced matrix compaction around the slurry-coated fibers or interference with the formation of a continuous contact layer at the fiber-matrix interface, both of which may limit mechanical interlocking and adhesion. Future research should focus on evaluating the long-term durability of fiber-reinforced earth mortars, particularly their resistance to moisture ingress, thermal cycling, and freeze-thaw conditions, as these factors are critical to ensuring structural integrity and service life in real-world applications. Furthermore, an important finding is that the sand content may be critical for applications requiring sufficient bond strength. Hence, further investigation is necessary to optimize the amount of sand needed. In addition, it is suggested that future studies evaluate long-term bond retention through accelerated ageing cycles and verify the effectiveness of treated fibers in full-scale 3D-printed wall panels.

This study contributes to the advancement of sustainable 3D printing technology by demonstrating that simple, low-cost fiber treatments and earth-based mortar formulations can significantly improve fiber-matrix bonding without the need for synthetic additives or complex processing – providing a viable pathway to environmentally friendly and locally adaptable construction solutions.

Acknowledgements

The first author, who was supported by the 2219 - International Postdoctoral Research Fellowship Program by the Scientific and Technological Research Council of Türkiye (TÜBİTAK) with grant number of 1059B192100924, expresses appreciation to TÜBİTAK.

Funding

The authors received no financial support for the research, authorship, and/or publication of this manuscript.

Conflict of Interest

The authors declared no potential conflicts of interest with respect to the research, authorship, and/or publication of this manuscript.

Author Contributions

All of the authors made substantial contributions to conception and design, or acquisition of data, or analysis and interpretation of data; were involved in drafting the manuscript or revising it critically for important intellectual content; and gave final approval of the version to be published.

Data Availability

The datasets created and/or analyzed during the current study are not publicly available, but are available from the corresponding author upon reasonable request.

REFERENCES

Abdeldjebar R, Hamouine A, Fouchal F, Labbaci B, Zebair A (2018). Effects of treated date palm fiber on durability of stabilized earth blocks (SEB). *International Journal of Civil Engineering and Technology*, 9(5), 293–305.

Abdi MR, Arjomand MA (2011). Pullout tests conducted on clay reinforced with geogrid encapsulated in thin layers of sand. *Geotextiles and Geomembranes*, 29(6), 588–595.

Alves Fidelis ME, Vitorino Castro Pereira T, da Fonseca Martins Gomes O, de Andrade Silva F, Dias Toledo Filho R (2013). The effect of fiber morphology on the tensile strength of natural fibers. *Journal of Materials Research and Technology*, 2(2), 149–157.

Archila H, Kaminski S, Trujillo D, Zea Escamilla E, Harries KA (2018). Bamboo reinforced concrete: A critical review. *Materials and Structures/Materiaux et Constructions*, 51, 1–18.

Benzerara M, Guihéneuf S, Belouettar R, Perrot A (2021). Combined and synergic effect of Algerian natural fibres and biopolymers on the reinforcement of extruded raw earth. *Construction and Building Materials*, 289, 123211.

Bulut H (2024). A different approach for green concrete production: Determination of the effect of e-waste and waste rubber powder on durability properties of concrete. *Challenge Journal of Concrete Research Letters*, 15(3), 69–81.

Dawood ZM, Alqaissi ZH (2024). Impact of date-palm fibers on fine soil's compaction and strength properties. *Journal of Engineering*, 30, 67–82.

EN ISO 17892-6 (2017). Geotechnical investigation and testing – laboratory testing of soil – Part 6: Fall cone test. European Committee for Standardization, Brussels, Belgium.

Fagone M, Kloft H, Loccarini F, Ranocchiai G (2019). Jute fabric as a reinforcement for rammed earth structures. *Composites Part B: Engineering*, 175, 107064.

Ferretti E, Moretti M, Chiusoli A, Naldoni L, de Fabritiis F, Visonà M (2022). Rice-husk shredding as a means of increasing the long-term mechanical properties of earthen mixtures for 3D printing. *Materials*, 15(3), 743.

Fode TA, Jande YA C, Kim YD, Ham MG, Lee J, Kivevele T, Rahbar N (2025). Effects of different lengths and doses of raw and treated sisal fibers in the cement composite material. *Scientific Reports*, 15(1), 1603.

Gomaa M, Jabi W, Veliz Reyes A, Soebarto V (2021). 3D printing system for earth-based construction: Case study of cob. *Automation in Construction*, 124, 103577.

Güney B, Yıldızel S (2024). Optimization of mechanical properties in lime-based composites using the Taguchi method. *Challenge Journal of Structural Mechanics*, 10(3), 109-115.

Lecompte T, Perrot A, Subrianto A, Le Duigou A, Ausias G (2015). A novel pull-out device used to study the influence of pressure during processing of cement-based material reinforced with coir. *Construction and Building Materials*, 78, 224–233.

Loccarini F (2017). Behaviour of Rammed Earth Structures: Sustainable Materials and Strengthening Techniques. *Ph.D.* thesis, University of Braunschweig, Braunschweig, Germany & University of Florence, Firenze, Italy.

Macherla URT (2023). A survey study on challenges and factors affecting in adopting sustainable construction methods in Indian construction industry. *MATEC Web of Conferences*, 384, 01004.

Mahmud H, Ahmed T, Islam MS (2025). Combined effect of rice husk ash and animal bone powder on strength and permeability of concrete. *Challenge Journal of Structural Mechanics*, 11(1), 1–13.

Melià P, Ruggieri G, Sabbadini S, Dotelli G (2014). Environmental impacts of natural and conventional building materials: A case study on earth plasters. *Journal of Cleaner Production*, 80, 179–186.

Mohamad N, Embong R, Othman NH, Muthusamy K, Jaafar MFM (2025). Flowability and compressive strength of ternary blended cement mortar of coal bottom ash and ground cockle shell ash. *Challenge Journal of Concrete Research Letters*, 16(1), 25–32.

Nagaraj HB, Muguda S (2020). Recent innovations in stabilized earthen construction. In: *Sustainable Materials in Building Construction*, Springer, Cham, 149–164.

Perrot A, Rangeard D, Pierre A (2016). Structural built-up of cement-based materials used for 3D-printing extrusion techniques. *Materials and Structures*, 49, 1213–1220.

Ramesh M, Palanikumar K, Reddy KH (2017). Plant fibre based bio-composites: Sustainable and renewable green materials. *Renewable and Sustainable Energy Reviews*, 79, 558–584.

Sen B, Saha R (2024). Structural stability evaluation of natural fiber retrofitted low-cost rammed earthen houses under seismic loading. *Structural Engineering International*, 35(2), 286–305.

Shahrubudin N, Lee TC, Ramlan R (2019). An overview on 3D printing technology: Technological, materials, and applications. *Procedia Manufacturing*, 35, 1286–1296.

Sposito S, Scalisi F (2017). Sustainable architecture: The eco-efficiency earth construction. *European Journal of Sustainable Development*, 6(4), 246–254.

Taallah B, Guettala A (2016). The mechanical and physical properties of compressed earth block stabilized with lime and filled with untreated and alkali-treated date palm fibers. *Construction and Building Materials*, 104, 52–62.

Tang CS, Shi B, Zhao LZ (2010). Interfacial shear strength of fiber reinforced soil. *Geotextiles and Geomembranes*, 28(1), 54–62.

Tarhan Y, Perrot A (2023). Reinforcement of 3D printable earth-based mortar with natural textile material. *Materials Today: Proceedings*, In Press.

Tarhan Y, Tarhan İH, Jacquet Y, Perrot A (2024). Mechanical behaviour of 3D printed and textile-reinforced eco-friendly composites. *Journal of Sustainable Cement-Based Materials*, 14(3), 477–495.

Yadav MEK, Kishore PR, Kumar AS, Swetha Sri AS (2019). Influence of sisal fibers on the properties of rammed earth. *International Journal of Innovative Technology and Exploring Engineering*, 8, 663–667.

Zavaleta D, Ñañez R, Silva G, Ruiz G, Pando MA, Aguilar R, Nakamatsu J, Kim S (2024). Additive construction using enhanced earthen-based composites: Improvement of the mechanical strength and water durability using chitosan and agave fibers. *Construction and Building Materials*, 411, 134159.

Challenge Journal of Structural Mechanics

Research Article

Examining the effects of different seismic base isolators on the seismic behavior of a real-size steel truss structure

Serdar Çarbaş [a], Refik Burak Taymuş [b,*], Mehmet Özdemir [a]

[a] *Department of Civil Engineering, Karamanoğlu Mehmetbey University, 70200 Karaman, Türkiye*
[b] *Department of Civil Engineering, Van Yüzüncü Yıl University, 65080 Van, Türkiye*

ABSTRACT

In this study, the seismic behavior of a real-size steel truss structure is examined for elastomeric isolator, double friction pendulum isolator, and fixed support conditions. Hence, the main aim of the study is to examine which type of support is safer for seismic response of a real-size steel truss structure, considering the structural reactions under earthquake and other acting load effects. To do this, the structural models generated with three different support conditions are examined in detail in terms of earthquake characteristic according to conducted structural seismic analyzes. The real-size steel truss structures are modeled in SAP2000 structural analysis program and are designed in accordance with the Turkish Building Earthquake Code-2018 specifications. The snow and wind loads acting on the truss structures are calculated in the direction of TS EN 1991-1-3 and TS EN 1991-1-4 specifications, respectively. The earthquake forces are implemented to the truss structure through mode superposition method. Finally, the truss structure is comparatively examined in terms of the structural weight, base shear force, natural vibration period, and relative drift. As regards to the obtained results, it has been observed that the seismic responses of the steel truss structure are remarkable better when the seismic base isolator is implemented into the structure.

ARTICLE INFO

Article history:
Received – April 14, 2025
Revision requested – May 12, 2025
Revision received – May 14, 2025
Accepted – May 27, 2025

Keywords:
Steel truss structure
Seismic response
Seismic base isolator
Double friction pendulum
Elastomeric isolator

Citation: Çarbaş S, Taymuş RB, Özdemir M (2025). Examining the effects of different seismic base isolators on the seismic behavior of a real-size steel truss structure. *Challenge Journal of Structural Mechanics*, 11(2), 106–115.

1. Introduction

Due to its geological location on numerous active faults, Türkiye is in high seismicity region. A large part of Türkiye is located within the earthquake zone formed by these faults. In other words, it is known that 95% of the population is under earthquake hazard and 98% of large industrial structures are located in these regions (Hattap and Eşsiz 2005). Because of country's location on such active faults, structural engineers have been conducted a lot of different construction design to resist on the earthquake behavior utilizing reinforced concrete and steel structures. Although steel structures are safer structural system due to the high strength and ductility of steel, their initial construction costs limit their usage in site. Hence, steel structures are preferably used in non-residential highway and railway bridges, industrial facilities, and/or low-rise buildings in Türkiye. Besides, the steel truss structural systems, which have recently started as to be in sports facilities, industrial buildings, stadiums, large shopping centers, concert and exhibition areas, etc., are a type of popular steel structure. The steel truss structures are designed based on the principle that structural elements are joined at the nodal points at which moments are zeroed and consequently, the elements forming the structure work only against axial ten-

* *Corresponding author*. Tel.: +90-432-225-1727 ; E-mail address: refikburaktaymus@yyu.edu.tr (R. B. Taymuş)
ISSN: 2149-8024 / DOI: https://doi.org/10.20528/cjsmec.2025.02.005

sion and compression forces. In terms of static benefits, these structures are much lighter than many other load-bearing structural systems, and the low dead loads reduce costs not only on the roof but also on the foundation and other sub-elements. Steel framed structures, on the other hand, are structures where column, beam, and floor structural elements are used, as in reinforced concrete structures. In such structures, column and beam elements have high bending stiffness, and connection points resist horizontal displacements. When designing seismic resilient construction, steel structures are generally preferred because of their low weight and high ductility. Since the structural weight of steel structures is approximately 50% less than that of reinforced concrete structures, the steel structures reacts to seismic forces at the same rate less (Özdemir 2022). Therefore, the damages caused by earthquakes in steel structures are less than other types of structures. Traditionally, steel structural systems are designed with the aim of damping the energies arising under earthquake loads by means of joints formed at the nodal points. In addition, seismic dampers are used in earthquake resistant steel structure designs in order to increase the stability of the structure under seismic effects. These are generally grouped as active and passive dampers. However, there are special hybrid damping systems that are formed by combining these two damping systems (Artar and Carbas 2022, 2023; Carbas and Artar 2024). Another effective method used to minimize the earthquake effect in steel structures is seismic isolation. Seismic isolation aims to minimize the earthquake damage to the structure by transferring the horizontal earthquake forces caused by the incoming ground motion to the superstructure as little as possible by means of so-called seismic isolator devices placed between the foundation and columns of the structure. The basic working principle of these isolator devices is to increase the period of the structure by increasing the horizontal displacement at the foundation of the structure. By increasing the period of the structure, the intensity of the spectral accelerations caused by the earthquake and the damaging effect of the earthquake in parallel are reduced as much as possible. Seismic base isolator systems differ in size, shape and especially in the material they are made of. The most commonly used ones are elastomeric isolators, lead-core isolators and friction pendulum isolators (Taymus 2021; Özdemir 2022). The usage of seismic isolation has become widespread in our country, as well. Scientific studies on seismic base isolation systems in our country have a substantial impact on the increase in practical applications (Özpalanlar 2004; Reyhanoğulları and Akyüz 2015; Wieland and Malla 2015; Erdem and Saifullah 2016; Erdem et al. 2016; Yurdakul and Yıldız 2020).

In this study, a steel truss structure was modeled in the SAP2000 structural analysis program according to three different support conditions (double friction pendulum isolator, elastomeric isolator, fixed support), and the seismic response of the structure under earthquake forces was investigated. It was also examined whether the application of seismic base isolators increases structural stability. The handled real-size steel truss structure originally designed with fixed supports and was constructed in the form of a tennis court, by implementing elastomeric isolators and double friction pendulum isolators under its load-bearing columns, resulting in a total of three different structural models. The main aim here is to examine in detail whether real-size steel truss structures can be constructed with less structural weight compared to traditional base design methods by placing different types of seismic base isolators, and most importantly, whether the seismic responses of the structure can be improved. For this purpose, the final structural designs were comparatively analyzed based on structural weight, base shear force, natural vibration period, and relative drift. Consequently, comparisons were made based on the results obtained for three different structural models; traditional fixed support, elastomeric isolator, and double friction pendulum isolator application.

2. Seismic Base Isolators

Seismic base isolators are one of the earthquake resilient systems that isolate the superstructure from the ground by separating it, thus reducing the reactions that may occur from ground motions and increasing the natural vibration period and damping ratio of the structure. They are one of the most effective seismic proof methods for minimizing the damage that seismic excitations can cause. They also play an important role in reducing both story drifts and story accelerations. In structures designed according to the traditional lateral load-bearing method, almost all acting loads originating from ground motions are transmitted to the superstructure, and the risk of these loads damaging the load-bearing elements is quite high. However, in seismically base-isolated structures, since energy absorption is high, the effect of external loads originating from ground motions on the superstructure is significantly less. When seismic isolators are used at the load-bearing columns' base in structural design, the structure initially exhibits an almost rigid behavior, and displacement occurs only in the isolators. As the natural vibration period of the structure increases, the spectral acceleration resulting from the earthquake and the deformation effect of the earthquake on the structure are significantly reduced. While the intensity of seismic forces originating from ground motions and acting on the structure may not be controlled, making the structure safer is achieved by reducing the intensity of the transmission of loads from the ground to the structure. The damping ratio, which is accepted as 5% in steel structures designed with normal traditional methods, increases up to 25% in structures where seismic base isolators are implemented (Kamrava 2015; Makris 2019; Taymus et al. 2024).

Various base isolator devices are used for seismic isolation. The most commonly used types are elastomeric and friction pendulum isolators (Kelly 2001; Naeim and Kelly 2007). The elastomer parts of elastomeric isolators are produced from natural rubber. One of the main reasons why they are preferred is that they can take the desired shape. They have good compatibility with metals and these features facilitate their installation on the

foundation in practice. Elastomeric isolators, which can deform up to four times the height of the rubber layers, have high stiffness vertically and very low stiffness horizontally (Fig. 1(a)). In the design and modelling stages of elastomeric isolators, especially their shear modulus, energy absorption capacity and time-dependent mechanical properties are expected to change as little as possible. In practice, they can be placed at the base of the column, in the middle of the column or between floors. In retrofitting projects, they can be used by creating a rigid platform between the column and the foundation. The working principle of friction pendulum isolators under earthquake loads is as follows; when the incoming seismic forces exceed the design friction force of the isolator, the steel sphere between the upper and lower plates starts to slide on the concavely designed lower plate and increases the oscillation period of the structure and makes the structure make small oscillations (Saiful Islam et al. 2011). In this way, the earthquake energy is damped by the friction force (Fig. 1(b)). Friction pendulum isolators can be designed in three different types: single, double, and triple friction pendulum.

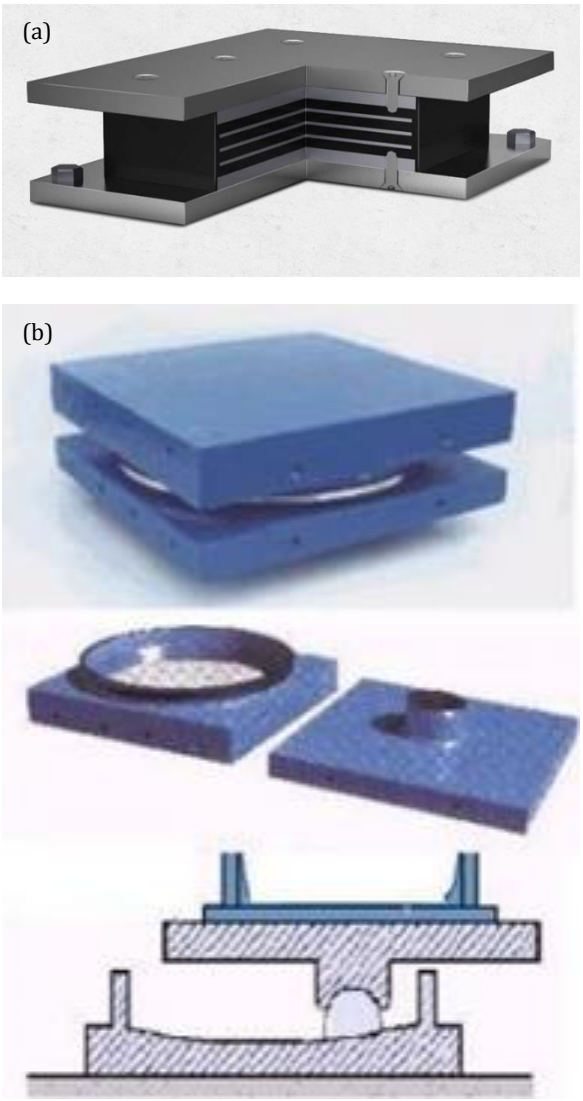

Fig. 1. Seismic base isolators: (a) Elastomeric (Arfen 2023); (b) Friction pendulum (Kan et al. 2017).

Among those triplets, the double friction pendulum isolator preferred in this study due to its popularity and ease of practicability is formed to consist of three components; the bottom and top plates, and the center slider. Such isolators are designed to absorb seismic energy by the movement of the center slider between the bottom plate and the top plate. Thus, a double friction surface is created that will be activated by the seismic loads coming to the structure. Since the friction will not be the same on two sliding surfaces, it is also considered that the sliding surface can always rotate a little. Therefore, the sliders are designed as articulated and irregular deformation is prevented. Since it has a double friction surface, it can be produced in smaller sizes and is often preferred in practice. Due to some rotation of the support body and the slider, this should be taken into account when calculating the displacement capacity. The double friction pendulum isolator cross-section and itself is shown in Fig. 2 (Constantinou 2004; Scheaua 2020).

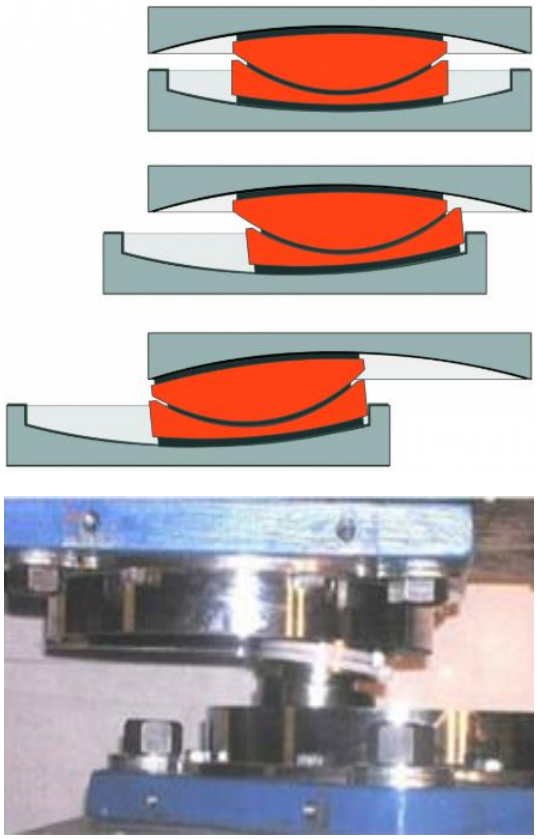

Fig. 2. Double friction pendulum isolators (Constantinou 2004; Scheaua 2020).

2.1. Modelling of elastomeric isolator in SAP2000

The elastomeric isolators can be modeled in SAP2000 structural analysis program. In this context, the ready-defined "Rubber Isolator" element type can used for this purpose. In elastomeric isolators, since there is no movement (sliding) limiter, a "gap" (clearance) definition is not made. After entering the mass and selecting the element orientations, data entries are made for the mechanical properties of the isolator. Since a nonlinear analysis

is performed, "NonLinear" must be selected and a "Stiffness" value is initially entered as 5025.313 kN/m. The "k1" value, which will be mentioned in the further section, is entered as the "Stiffness" value. The "Yield Strength" value is also entered as the force value of 92.4658 kN at which the "k2" value starts. The value of the "k1/k2" ratio is entered as the "Post-yield Stifness Ratio" value as 0.1667. The "Rubber Isolator" option readily available in the SAP2000 structural analysis program, as mentioned before, this type of isolator can also be modeled by selecting a single "Link" element. In fact, the "Rubber Isolator" used here is a biaxial hysteretic isolator that exhibits plastic behavior for orthogonal and interactive shear deformations in two directions and shows linear effective stiffness for the other four deformations. The hysteretic concept in this definition is the cyclic response behavior exhibited by the internal force-deformation relationship formed in the element as a result of external seismic loading. For each shear deformation degree of freedom, linear or nonlinear behavior can be defined (Özpalanlar 2004). When modeling the elastomeric isolator in the SAP2000 structural analysis program, a "Link" element definition is initially made downwards from the connection point of the structure with the foundation. A fixed end support is assigned to the bottom point of the defined "Link" element. The defined "Rubber Isolator," as explained above, is assigned to this "Link" element. The visuals of the elastomeric isolators modeled in the SAP2000 structural analysis program are shown in Fig. 3.

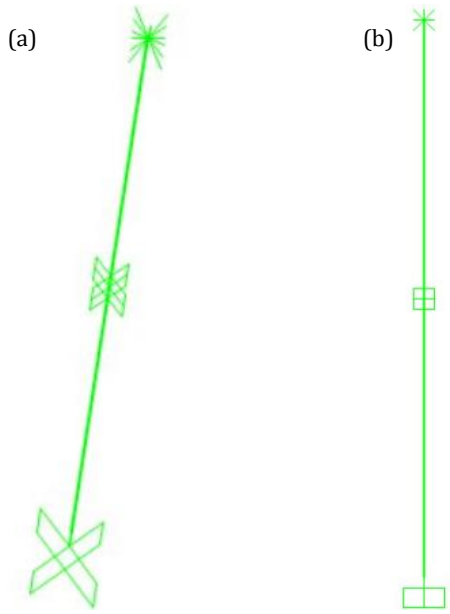

Fig. 3. Elastomeric isolator modeled in SAP2000: (a) 3D view; (b) x-z plane view.

2.2. Modelling of double friction pendulum isolator in SAP2000

Within the scope of this study, the double friction pendulum isolator has been modeled in the SAP2000 structural analysis program by utilizing “Plastic (Wen)” option as link/support data. The elements to be defined as "Plastic (Wen)" are considered as plastic hinges. Also, a gap is defined in the form of a "gap" element. Namely, the element definitions have been made as "Plastic (Wen)," i.e., plastic hinge, and "gap," i.e., gap element. All solutions made other than the "NonLinear Link" element definition is calculated assumed as linear behavior. Another data entry is made to define the orientations and mechanical properties. Here, for mechanical properties, the "Effective Stiffness" and "Effective Damping" properties to be used in "Linear" analysis are entered. Then, the element properties "Stiffness" and "Open" to be used in "Nonlinear" analysis. The selected "U1" direction means to make a definition equivalent to the x-direction in the coordinate system if the global axis system is defined in the SAP2000 structural analysis program. Later, the mechanical values of the "gap" element are entered. When modeling the double friction pendulum isolator, it should be taken into account that it will move horizontally and slide, and when it displaces to the edges of the concave surface, it should not displace further due to the limiters at the edges of this surface. So, the isolator has a certain displacement capacity. In the "gap" element, this represents the displacement capacity. In the SAP2000 structural analysis program, the "Open" option is defined as the displacement capacity. The "Stiffness" option represents the bearing capacity stiffness of the isolator after it displaces up to the limiters. Naturally, this value should be entered as a large value that will prevent deformation during isolator modeling. The assumption that the "Effective stiffness" value is 1/500th of the normal "Stiffness" value can be accepted. After mass definition, the "U2" and "U3" directions are selected. To define the properties of these directions, the "Stiffness" value is entered as the stiffness value in the nonlinear analysis. Thereby, the double friction pendulum isolator will not displace, i.e., will not move, until the friction force is reached. When making the "Plastic (Wen)" element definition, calculations are made assuming very high stiffness and a slight amount of displacement. The "Yield Strength" value is the force value at which sliding, i.e., yielding, begins. In this study, since a simulation is performed and to be exactly the same in reality, the "Plastic (Wen)" element type was used when modeling the double friction pendulum isolator. The "Post Yield Stiffness Ratio" value is defined as the ratio of the stiffness at the moment yielding starts to the stiffness after yielding ends. The "Yielding Exponent" value is generally taken as 22. In Friction Pendulum Bearings, transitions between sliding regimes occur sharply. The Yielding Exponent parameter should be a value that reveals this sharpness. Thus, the reason for taking "Yielding Exponent" value as 22 is that the hysteretic curve of double friction pendulum isolators should be sharply cornered, i.e., square or rectangular in shape. Here, the larger the area under the curve, the more the energy damping capacity against earthquake effects for steel structures is increased.

When modeling the double friction pendulum isolator in the SAP2000 structural analysis program, first, the concave surface of the lower part of the isolator is considered, and 5 “link” element definitions are made. This element type is defined to the start, end, and joint points of the "Link" elements. Then, fixed supports are defined

at the corner points. Displacement of the bottom 5 points of the isolator is prevented. In the upper part of the isolator, movement under seismic forces is considered. The upper part of the isolator also has 5 "link" element definitions just like the bottom, and this element type is defined to the start, end, and joint points of these elements. The "Plastic (Wen)" link element is assigned to the defined vertical links, and the "gap" link elements are assigned to the horizontal links. Since the three points defined on the upper plate of the isolator will not move independently, it is assumed that they will move together. Hence, "Joint constraints" are defined and assigned to these 3 points in the SAP2000 structural analysis program. The 2 points in the middle of the lower and upper plates represent the central slider. Since it is assumed that these two points will move together, "joint constraints" have been assigned. However, different "joint constraints" have been assigned to the 3 points on the upper plate and the 2 points on the lower plate. The reason for this is that the upper 3 points and the middle 2 points need to move separately. The "joint restraints" assignment to the top middle point of the upper plate is made. Since the points on the upper plate will move together, assignment has been made only to this point. The double friction pendulum isolators modeled in the SAP2000 structural analysis program are shown in Fig. 4.

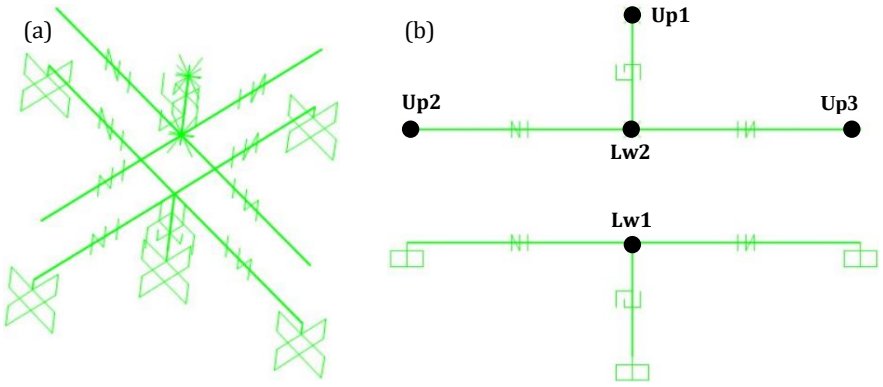

Fig. 4. Double fraction pendulum isolator modeled in SAP2000: (a) 3D view; (b) x-z plane view.

3. Design of Real-Size Steel Truss Structure in SAP2000 using Seismic Base Isolators

With the nonlinear analysis capability developed in the SAP2000 structural analysis program, the static and dynamic computations and designs of real-size (3D) steel truss structures can be performed by defining nonlinear elements. According to Hooke's law, there should be a linear displacement according to the applied force. However, in nonlinear analysis, the applied force and displacement do not change linearly. The element may flex or deform without flexing under the applied force. Therefore, nonlinear analysis should also be performed in the design of steel structures. This type of analysis performed in steel structure design is called second-order analysis. From this point of view, it is understood that linear displacement occurs in linear analysis under force, and nonlinear displacement occurs in nonlinear analysis. The type of material used is also important in this respect. The resistance shown by the material against force, that is, its yield strength, may not be clear after it is exceeded. In this case, the hardness or stiffness value of the material used play very significant role. Therefore, these values should be considered in the calculations in duration of design. One of the reasons for performing nonlinear analysis during design is that as the force effect increases in linear analysis, the sections in the design grow at the same rate, but in nonlinear analysis, the structure can be designed with smaller cross-sections (Özdemir 2022).

In this study, a real-size steel truss structure taken as a structural design example was modeled with 7 span, each span has 6 m wide, and a truss span of 21 m. The 3D view of the modelled real-size steel truss structure is shown in Fig. 5. The columns of the structure were designed using Q1685mm pipe profiles, the roof trusses using Q1684mm pipe profiles, the column bracing members using Q763mm pipe profiles, the roof truss bracing members using 603mm pipe profiles, the roof purlins using 40x80x3 mm box profiles, and the bracing members also using 40×80×3mm box profiles. In this study, the snow and wind loads acting on the life-size steel truss structure were calculated by considering the criteria in TS EN 1991-1-3 (2025) and TS EN 1991-1-4 (2022) specifications regulations, respectively.

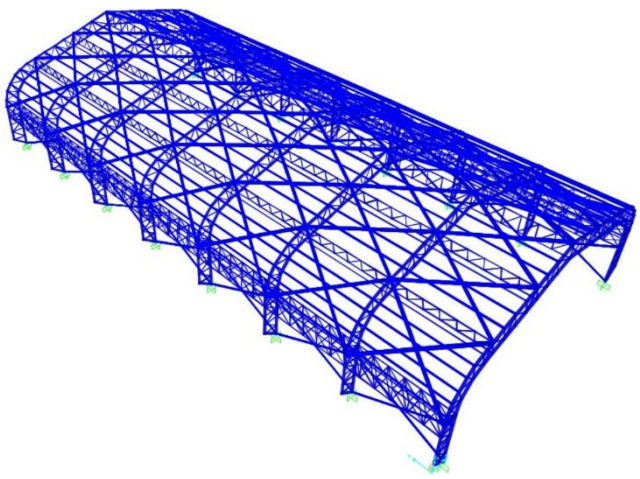

Fig. 5. 3D view of real-size steel truss structure modeled in SAP2000.

3.1. Seismic data identification using mode superposition method

In this study, it was assumed that the real-size steel truss structure taken as a design example would be constructed in Karatay/Konya at coordinates latitude '37.88680' and longitude '32.500621'. Based on these coordinates, an earthquake hazard report and a horizontal elastic design spectrum were generated from the website of the Disaster and Emergency Management Presidency (AFAD) (Fig. 6).

The data considered when creating the spectrum above were selected as Ss=0.686, S_1=0.148, S_{DS}=0.841, S_{D1}=0.222, PGA=0.293, PGV=14.219, and soil class ZD. Afterwards, a reduced design spectrum graph was created by considering the horizontal elastic design spectrum. The reduced design spectrum graph was graphed according to the earthquake load reduction factor design criteria under the title "Earthquake Load Coefficients and Capacity Design Principles" from the Türkiye Building Earthquake Code-2018 (TBEC 2018) as depicted in Fig. 7. Here, R=4 and D=2 are taken from TBEC-2018/Table 4.1, I=1.2 is taken from TBEC-2018/Table 3.1, $TB=S_{D1}/S_{DS}$ is taken from TBEC-2018/Eq. 2.3 and so the TB=0,264 is calculated.

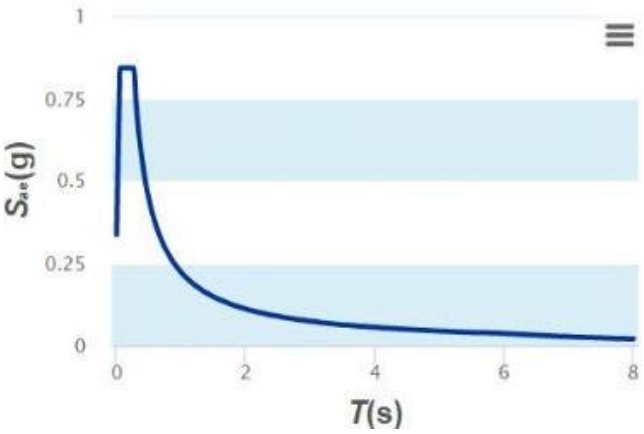

Fig. 6. Horizontal elastic design spectrum graph.

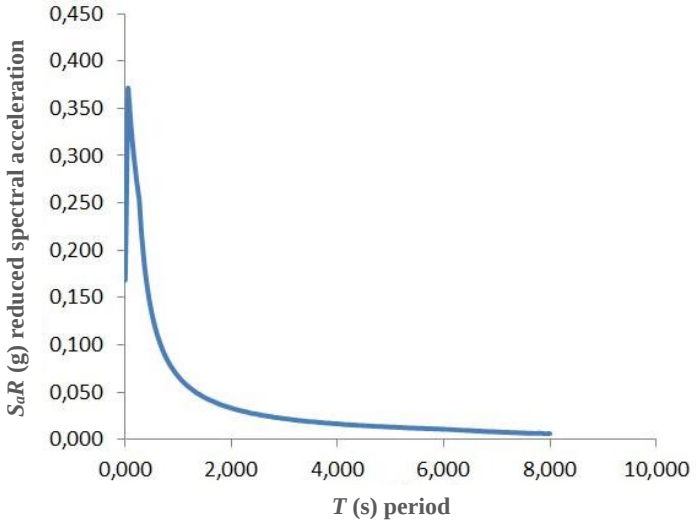

Fig. 7. Reduced response design spectrum graph.

The reduced response design spectrum was created according to the design criteria in the relevant section of TBEC-2018. The method used in this study is the mode superposition method, which is one of the dynamic solution methods. The mode superposition method is solved by statistically combining the maximum internal forces and displacements calculated for each of the natural vibration periods in the structure (İşsever 2012). From the equations under the title "4.2.1. Earthquake Load Reduction Factor" of TBEC-2018;

$$R_a(T) = R \quad \text{for} \quad T > TB \tag{1}$$

$$R_a(T) = D + (R - D) \cdot \frac{T}{TB} \quad \text{for} \quad T \leq TB \tag{2}$$

$$S_aR(T) = \frac{S_{ae}(T)}{R_a(T)} \quad \text{for} \quad T > TB \tag{3}$$

In these equations;
S_aR(T): reduced spectral acceleration for a specific natural vibration mode,
S_{ae}(T): elastic spectral acceleration for a specific vibration mode,
R_a(T): earthquake load reduction factor for a specific vibration mode.

Subsequently, the period, elastic design spectrum values, earthquake load reduction factor, and reduced accelerations were created in an Excel program and saved as a ".txt" extension file compatible with the SAP2000 structural analysis program. In the SAP2000 structural analysis program, "Function" was entered from the "Define" tab, and then "Response Spectrum Function Definition". Then, the created ".txt" format text document was loaded to crate the response spectrum function graph. The reduced response spectrum graph through the "Load Case Data" tab was defined in the SAP2000 structural analysis program and included in the structural analysis. While identification the data, real acceleration-time records were applied to the structure in both directions in accordance with the TBEC-2018 specifications.

3.2. Modal analysis

It is important to consider modal analysis when making structural designs. This is because most structures tend to vibrate at natural frequencies even when not under any load or force. Due to these natural frequencies, structures exhibit mode changes, even if very slightly. This type of analysis is used to determine the parameters needed to define the design that shows the dynamic behavior of structures. In this way, the created modes, natural frequency, damping, and resulting mode shapes can be determined. If modal analysis is categorized, it can be divided into traditional modal analysis and operational modal analysis. If the vibrations to be applied to the structure are known, the conventional modal analysis method can be used. However, if the vibrations to be applied to the structure are unknown, the operational modal analysis should be preferred. During the analysis, it is assumed that the structure is a whole, its structural behavior does not change over time, the material properties do not change, and the structure exhibits linear characteristic (Şahin et al. 2020). Fig. 8 below shows the behavior of the real-size steel truss structure subjected to modal analysis in the SAP2000 structural analysis program at "mode=1".

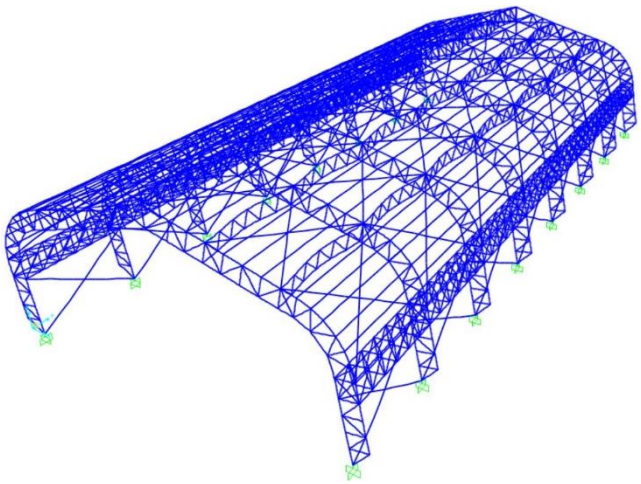

Fig. 8. View in x-z plane of real-size steel truss structure as a result of modal analysis via SAP2000.

4. Discussions

In this study, a real-size steel truss structure modeled in the SAP2000 structural analysis program was first designed using the traditional base method, i.e., with fixed supports. Then, the structure was designed separately again for the cases elastomeric and double friction pendulum seismic base isolators. Consequently, the structural analyses of three different structural design models—fixed supported, with elastomeric seismic base isolators, and with double friction pendulum seismic base isolators—under the load effects were carried out. The obtained structural design solutions were then examined in terms of comparisons of structural weights, base shear forces, natural vibration periods, and relative drifts.

In order to compare the structural weight of the life-size steel frame structure modeled with and without seismic base isolator using SAP2000 structural analysis program, the obtained weight of structures from each structural analysis for the cases with fixed support, elastomeric isolator, and double friction pendulum isolator are tabulated in Table 1. The total reaction weight of the structure was calculated by summing the reaction force values occurring at the supports. When Table 1 is examined, it is seen that the highest reaction force occurs when implementation of the elastomeric isolators, followed by the case where double friction pendulum isolators are implemented, and the lowest reaction force occurs when implementation of fixed supports. When the steel truss structure is designed with double friction pendulum isolators, it gives approximately 60% higher reaction force compared to the case where it is designed with fixed supports.

When the base shear forces of the real-size steel truss structure designed with and without isolators using SAP2000 structural analysis program are compared it can be deducted that considering the resistance of the real-size steel truss structure modeled in the SAP2000 structural analysis program against seismic effects, the values of shear forces play an important role in determining the section properties. As can be understood from the base shear force values resisted by the supports shown in Fig. 9, the highest base shear force is resisted by elastomeric isolators, followed by double friction pendulum isolators, and the lowest by fixed supports.

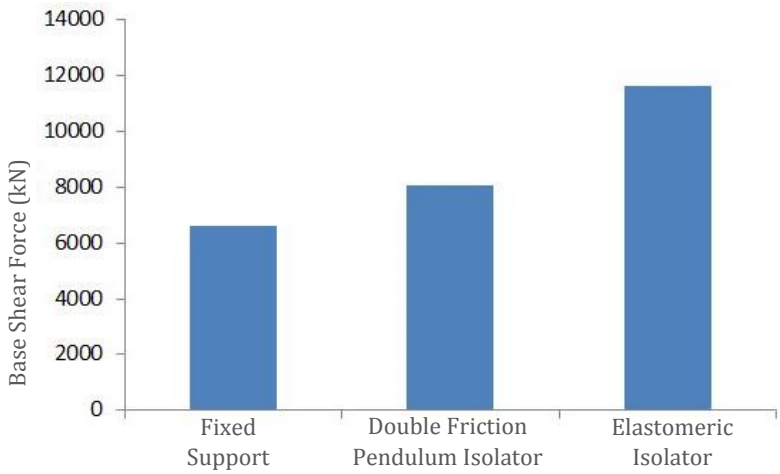

Fig. 9. Base shear forces with respect to support conditions.

Table 1. Structural weights with and without seismic base isolator.

P_{total}/Fixed Support (kN)	P_{total}/Elastomeric Isolator (kN)	P_{total}/Double Friction Pendulum Isolator (kN)
7.583,81	8.215,29	12.058,17

When Fig. 9 is examined, it is seen that the elastomeric isolator resists approximately twice as much base shear force as the fixed support when used in the real-size steel truss structure. When the double friction pendulum isolator is implemented in the real-size steel truss structure, it is seen that it resists approximately 20% more base shear force compared to the fixed support as obviously seen in Table 2.

Table 2. Base shear forces for the support condition according to load combinations.

Support Condition	Fixed Support	Double Friction Pendulum Isolator	Elastomeric Isolator
Maximum base shear force according to load combinations	V_{Max} (kN)	V_{Max} (kN)	V_{Max} (kN)
1.2G+0.2S+Ex	6.644,38	–	–
1.2G+0.2S+Ey	–	8.056,55	–
1.2G+0.2S+Ex	–	–	11.623,03

In Table 2, the maximum base shear force obtained from the structural analysis results executed in the SAP2000 structural analysis program according to the load combinations are given. Here, while maximum base shear force values are obtained in the 1.2G+0.2S+Ex load combination when fixed support and elastomeric isolator are implemented into the structure, the maximum base shear force value is obtained in the 1.2G+0.2S+Ey load combination when double friction pendulum isolators are implemented into the structure. When the isolated steel truss structures are compared among themselves, it is seen that approximately 47% more base shear force is resisted in the case where elastomeric isolators are implemented into the structure compared to the case where double pendulum isolators are implemented.

The natural vibration periods obtained for the first, second, and third structural modes as a result of the structural analyses of the real-size steel truss structure modeled with fixed supports and seismic base isolators in the SAP2000 structural analysis program are tabulated in Table 3.

Table 3. Natural vibration periods according to support conditions.

Structural Modes	$T_{\text{fixed support}}$ (sec)	$T_{\text{double friction pendulum isolator}}$ (sec)	$T_{\text{elastomeric isolator}}$ (sec)
1	0.23	0.29	0.41
2	0.11	0.21	0.38
3	0.10	0.11	0.13

If Table 3 is examined, it is seen that the natural vibration period of the real-size steel truss structures increases by approximately two times of magnitude when designed with base isolators compared to the case where they are designed with fixed supports. After the third mode, it is seen that the natural vibration periods of the structure reach almost the same values for all support conditions.

After the structural analyses of the real-size steel truss structures modeled with fixed supports, double friction pendulum isolators, and elastomeric isolators in the SAP2000 structural analysis program, the maximum relative drifts were obtained when the relative drifts at the apex points of the trusses and the relative drifts at the internal joint points where the fully vertical truss members end and the inclined truss members begin, which are in the same alignment as the fixed supports/isolators, were considered. The maximum relative drifts values of the obtained results are tabulated in Table 4. It is seen that the maximum relative drifts obtained for the fixed supported structural case will be greater than the relative drifts obtained in the cases where the structure is modeled with isolators. The maximum apex point relative drift was obtained in the 1.2G+0.5S+1.6Wy load combination for the isolated structural designs, and in the 1.2G+0.2S+Ex load combination for the fixed supported structural design. On the other hand, the relative drift values at the internal joint points where the fully vertical truss members end and the inclined truss members begin, which are in the same alignment, were obtained from the 1.2G+0.5S+1.6Wy load combination for the isolated structural designs, and from the 1.2G+0.2S+Ex load combination for the fixed supported structural design.

Table 4. Relative drifts of the apex point and specified joints for three different support conditions according to load combinations.

Support Condition	Fixed Support	Double Friction Pendulum Isolator	Elastomeric Isolator
Maximum relative drifts according to load combinations	$\Delta apex_{max}$ / $\Delta joint_{max}$ (cm)	$\Delta apex_{max}$ / $\Delta joint_{max}$ (cm)	$\Delta apex_{max}$ / $\Delta joint_{max}$ (cm)
1.2G+0.5S+1.6Wy	–	(1.88) / (1.87)	(1.87) / (1.78)
1.2G+0.2S+E_X	(4.3) / (4.27)	–	–

When Table 4 is examined, it is seen that maximum relative drifts at the apex point and at the internal joints, which are in the same alignment as the isolators, where the fully vertical truss members end and the inclined truss members begin, were obtained in the same load combination and in the same direction (*y*-direction) for the isolated structural designs. It has been observed that the maximum relative drift value in the steel truss structure with fixed supports is greater than the maximum relative drift values in the seismically isolated structures. In this context, the structures with seismic isolators exhibited approximately 40% less maximum relative drift compared to the structure with fixed supports. When the seismic isolated structural cases are compared within themselves, almost the same relative drift values were obtained (Fig. 10).

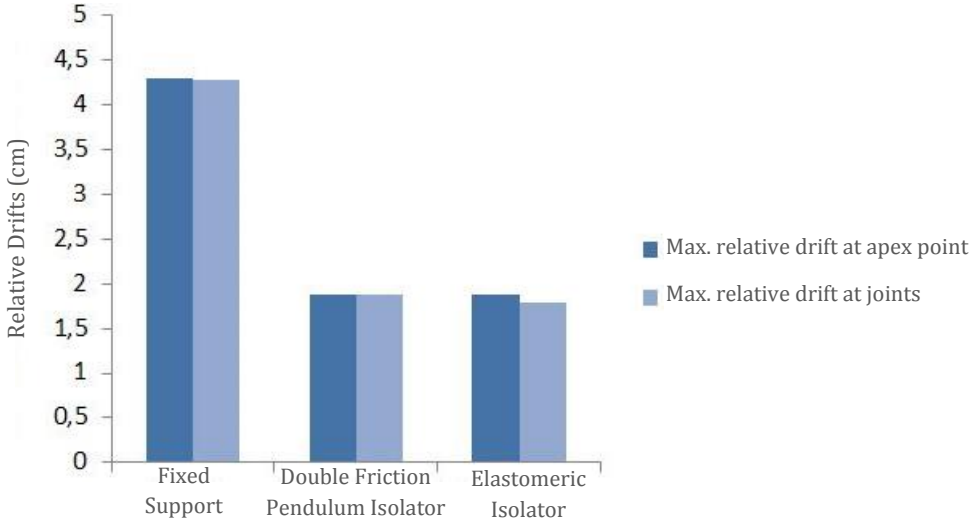

Fig. 10. Comparison of relative drifts according to support conditions.

5. Conclusions

In this study, to investigate the seismic response characteristic of a real-size steel truss structure, the structure was modeled and designed in SAP2000 structural analysis program according to a total of three different support conditions as fixed support, double friction pendulum isolator, and elastomeric isolator. The structural analyses were performed according to the mode superposition method. The achieved structural analysis of real-size steel truss structures were compared in regard of the structural weight, base shear force, natural vibration period, and relative drifts. Thus, in this study, the seismic response characteristic of the real-size steel truss structures with seismic base isolation and a steel truss structure modeled with traditional fixed supports against earthquake forces was investigated. Within the scope of this study, the following main concluding remarks were deducted:

- Considering the structural weight calculated according to the support reaction forces obtained from the structural analysis results, fixed supported and seismically isolated steel truss structures were compared, and the results are given in Table 1. According to this table, it has been observed that the fixed supported steel truss structure gives a lower reaction force value compared to the seismically isolated structures. In the comparison made according to the base shear force, it is seen that the steel truss structures with seismic base isolators resist a higher base shear force, and therefore, more resilient structural systems against earthquake effects are constructed. This is because a large part of the seismic energy coming into the structure during the completion of the oscillation of the steel truss structures is damped by the seismic base isolators implemented into the structure, so the base shear force has reached its maximum value. In addition, when a comparison is made according to the maximum relative drifts obtained, the drift values in the structure are also low due to the isolators becoming active when the structure starts to oscillate under the influence of seismic forces. From these results, it

is seen that real-size steel truss structures with seismic base isolation become safer against earthquake forces. In other words, it is seen that steel truss structures exhibit effective seismic resilience performance against earthquake forces when they are designed with properly modeled seismic base isolations.

- The most important result obtained mainly in this study is that when seismic base isolators are used practically in real-size steel truss structures, loss of life and damage will be prevented due to the structure exhibiting effective seismic performance against earthquake forces.

Acknowledgements

The results presented in this study are mostly based on the M.Sc. thesis titled "Seismic Response Investigation of Real Size Steel Truss Structure by Implementing Various Types of Seismic Isolators" at Karamanoğlu Mehmetbey University, Karaman, Türkiye, 2022, which is gratefully acknowledged.

Funding

The authors received no financial support for the research, authorship, and/or publication of this manuscript.

Conflict of Interest

The authors declared no potential conflicts of interest with respect to the research, authorship, and/or publication of this manuscript.

Author Contributions

All of the authors made substantial contributions to conception and design, or acquisition of data, or analysis and interpretation of data; were involved in drafting the manuscript or revising it critically for important intellectual content; and gave final approval of the version to be published.

Data Availability

The datasets created and/or analyzed during the current study are not publicly available, but are available from the corresponding author upon reasonable request.

REFERENCES

Arfen (2023) Bridge Expansion Joints and Bearings & Slab Joint. In: Bridg. Mov. Profiles Bear. Slab Jt. http://www.arfen.com/Kopru-Genlesme-Profilleri.asp?LanguageID=2&cid=3&id=1013 [accessed 02.04. 2025].

Artar M, Carbas S (2022). Optimum sizing design of steel frame structures through maximum energy dissipation of friction dampers under seismic excitations. *Structures,* 44, 1928–1944.

Artar M, Carbas S (2023). Optimizing the seismic resilience performance of steel truss bridges by maximum energy dissipation via friction dampers. *Structures,* 58, 105508.

Carbas S, Artar M (2024). Optimum steel frame design through ultimate seismic energy dissipation of double diagonal friction dampers. *Structures,* 60, 105964.

Constantinou MC (2004). Friction Pendulum Double Concave Bearing. NEES Report, Buffalo, New York, USA.

Erdem S, Saifullah K (2016). Soft-story effects on the behaviour of seismically isolated buildings under near and far-fault earthquakes. *Challenge Journal of Structural Mechanics*, 2(4), 234–245.

Erdem S, Saifullah K, Gürbüz E, Blankson MA (2016). The influence of different concrete classes on the seismic response of a seismically isolated building. *Challenge Journal of Structural Mechanics,* 2(3), 169–178.

Hattap S, Eşsiz Ö (2005). Depreme karşı çelik konstriksiyon. In: *Deprem Sempozyumu*, Kocaeli, Türkiye, 950–959. (in Turkish)

İşsever MA (2012). Comparing of Equivalent Seicmic Load Method and Mode Superposition Method on Multi-Story Reinforced Concrete Building. *M.Sc. thesis*, İstanbul Technical University, İstanbul, Türkiye.

Kamrava A (2015). Seismic isolators and their types. *Current World Environment*, 10, 27–32.

Kan Ö, Kaymaz K, Zengin B, Özcan M (2017). Investigation of seismic isolation types of earthquake resistant structures in Türkiye. *Bilim ve Gençlik Dergisi*, 5, 83–100.

Kelly TE (2001). Base isolation of structures: design guidelines. In: Auckl. Holmes Consult. Gr. Ltd. www.holmesgroup.com [accessed 05.04.2025].

Makris N (2019). Seismic isolation: Early history. *Earthquake Engineering and Structural Dynamics*, 48, 269–283.

Naeim F, Kelly J (2007). Design of Seismic Isolated Structures: From Theory to Practice. John Wiley and Sons Inc.

Özdemir M (2022). Seismic Response Investigation of Real Size Steel Truss Structure by Implementing Various Types of Seismic Isolators. *M.Sc. thesis*, Karamanoğlu Mehmetbey University, Karaman, Türkiye.

Özpalanlar CG (2004). Seismic Isolation and Energy Dissipating Systems in Earthquake Resistant Structural Design. *M.Sc. thesis*, İstanbul Technical University, İstanbul, Türkiye.

Reyhanoğulları NE, Akyüz U (2015). Vertical ground motion influence on seismically isolated & unisolated bridges. *Challenge Journal of Structural Mechanics*, 1(3), 117–123.

Şahin M, Okuyucu D, Şahin B, et al. (2020). Evaluation of vibration measurement setups for operational modal analysis of a base isolated structure. In: *4. Uluslararası GAP Matematik-Mühendislik-Fen ve Sağlık Bilimleri Kongresi*, Gaziantep, Türkiye, 73–85.

Saiful Islam ABM, Jameel M, Jumaat MZ (2011). Seismic isolation in buildings to be a practical reality: Behavior of structure and installation technique. *Journal of Engineering and Technology Research*, 3, 99–117.

Scheaua F (2020). Improvement of structures seismic response based on pendulum systems with double sliding surface. *IOP Conference Series: Materials Science and Engineering*, 916.

Taymus RB (2021) Optimum Design of Seismic Isolated Steel Construction Buildings with Triple Friction Pendulum Bearings. *Ph.D. thesis*, Akdeniz University, Antalya, Türkiye.

Taymus RB, Aydogdu I, Carbas S, Ormecioglu TO (2024). Seismic design optimization of space steel frame buildings equipped with triple friction pendulum base isolators. *Journal of Building Engineering*, 92, 109748.

TBEC (2018). Turkish Building Earthquake Code-2018. Rebublic of Türkiye Minister of Environment, Urbanisation and Climate Change, Ankara, Türkiye.

TS EN 1991-1-3 (2025). Eurocode 1 – Actions on structures – Part 1-3: Snow loads. Turkish Standards Institution, Ankara, Türkiye.

TS EN 1991-1-4 (2022). Eurocode 1 – Actions on structures – Part 1-4: General actions – Wind actions. Turkish Standards Institution, Ankara, Türkiye.

Wieland M, Malla S (2015). Earthquake design of a viaduct with full seismic isolation of bridge deck. *Challenge Journal of Structural Mechanics*, 1(1), 27–31.

Yurdakul M, Yıldız MB (2020). A study on seismic isolation of building used LRB. *Challenge Journal of Structural Mechanics*, 6(2), 52–60.